Chapter 13

GeO_2 Films with Ge-Nanoclusters in Layered Compositions: Structural Modifications with Laser Pulses

Evgenii Gorokhov, Kseniya Astankova, Alexander Komonov and Arseniy Kuznetsov

Additional information is available at the end of the chapter

http://dx.doi.org/10.5772/53481

1. Introduction

In this chapter, we will discuss issues related to the development of new materials and device technology for micro-, nanoelectronics and optics. More specifically, our research activities were devoted to the study of objects in which 3D quantum size effect was revealed. These are a group of materials consisting of indirect-band-gap semiconductor nanoclusters embedded in insulator (Knoss, 2008; Molinari et al., 2003; Takeoka et al., 1998).

Changes in the optical properties of Ge-nanoclusters due to 3D quantum size effect in metastable germanium monooxide (GeO(solid)) layers after decomposition of such layers into Ge and GeO_2 (GeO_2<Ge-NCs>) were observed by us as early as in the late seventies, i.e. a few years before this effect was for the first time reported in the literature (Ekimov & Onuschenko, 1981). It should be emphasised here that in our experiments this effect was observed in a thin-film heterosystem rather than in bulk SiO_2 glasses with CuCl or CdS precipitates. The latter circumstance is important for using such materials in modern film technology of micro-, nano- and optoelectronics.

Apart from the detection of the photoluminescence coming from GeO_2<Ge-NCs> heterolayers, we showed that the 3D quantum size effect, radically changing the properties of the electron subsystem of the solid, could also be used to achieve a dramatic modification of the lattice subsystem of the solid matter. So, a new material, nanofoam, a solid similar to aerogels (Hrubesh & Poco, 1995), was obtained from germanium dioxide in GeO_2<Ge-NCs> heterolayers (Gorokhov et al., 2011). Simultaneously, we have developed a new technique allowing easy production of Ge-quantum dots (Ge-QDs) of a very small size. The dispersion of QDs sizes in obtained GeO_2<Ge-NCs> layers could be significantly reduced in comparison with the dispersion of Ge-QD sizes in GeO_2<Ge-NCs> heterolayers.

In our work, thin films from the following germanium oxides were investigated:

1. GeO(solid) films, which were layers of (usually amorphous) stoichiometric germanium monooxide (also, there are reported data about the existence of crystalline modifications of GeO(solid) (Martynenko et al., 1973));
2. GeO_x films, which were nonstoichiometric GeO(solid) layers with x, standing to indicate the chemical composition of the material, ranging in $0 < x < 2$ (I) or $1 < x < 2$ (II). In case I, the composition of GeO_x varies from pure germanium to GeO_2, and in case II, it varies between the stoichiometric compositions of GeO(solid) and GeO_2;
3. GeO_2 films, which can be amorphous or have crystalline modifications;
4. heterogeneous material GeO_2<Ge-NCs>, obtained from metastable GeO(solid) during its chemical decomposition into two components: an amorphous GeO_2 matrix and Ge-nanoclusters dispersed throughout the matrix.

These film materials, belonging to dielectrics, were recognised inappropriate for use in planar Si-based IC technology, and they were therefore forgotten. The main reason was that germanium monooxide was a metastable material readily undergoing decomposition even without any additional heating (Marin, 2010). Second, the layers of amorphous germanium dioxide rapidly dissolve in water (Kamata, 2008). Therefore, layers of amorphous GeO(solid) and GeO_2 were recognised inferrior to thermal silicon dioxide films, as well as to high-temperature silicon nitride films, which also proved to be chemically resistant and mechanically strong. In addition, it was absolutely unclear how patterning or selective etching of germanium oxide layers could be achieved. Other layers of germanium oxides, such as hexagonal GeO_2 and GeO_2<Ge-NCs> heterolayers, were unknown at that time when the possibility of using germanium oxide films in semiconductor industry was under evaluation. Also, there were no reported data on the interaction of layers of amorphous GeO_2 with SiO_2 or Si_3N_4 and on subsequent crystallisation of such binary compositions (Gorokhov et al., 1987, 1998).

However, the study of properties and specific features of all modifications of film compounds based on germanium oxides have led us to a revision of the appropriateness of such compounds for use in modern technology of solid-state devices in micro-, nano- and optoelectronics. The main advantage of germanium oxide layers over other dielectric layers consists in the capability of such layers (both atomic and electronic subsystem) to be easily modified during treatments given to the layers, and the modifications lead to a significant change of the initial properties of the material. Therefore, a deposited film of germanium oxides should now not be considered as a fully complete and final result of some process sequence; instead, it should be considered as a material suitable for subsequent modifications. In particular, based on such layers, one can create light-emitting diodes, photodiodes, optoelectronic couples, optical fibers, interference filters, mirrors, lenses, diffraction gratings and holograms, as well as single electron transistors, memory elements, resists for laser and probe nanolithography, low-k and high-k dielectrics, and a component of colloidal solutions of Ge-nanoparticles to fight against cancer in medicine (Tyurnina et al., 2011). To date, not all device applications of germanium oxide layers have been identified.

From our point of view, the specific properties of germanium oxide compounds outlined above show great promise in the development of the nanotechnology of layered systems in nanoelectronics. A pressing problem in this field is developing methods for local modification of film coatings aimed at imparting desired properties to a small area of the film only. Especially, there is a problem of formation of elements having extremely small sizes in one or two dimensions in a thin continuous planar layer.

Studying the potential offered by narrow linear and dot scanning laser treatments as applied to thin-film materials or surfaces exhibiting photosensitivity or susceptible of high-intensity focused laser radiation, i.e. laser micro- and nanolithography, was one of the promising research lines at this topic. A big volume of research has been done by us in this field, and that has brought forth many interesting effects and successful developments. Achievement of modification effects in thin near-surface layers of substance while leaving the material intact at larger depths is another research area in using laser treatments in micro- and nanoelectronics. Local modifications of material properties could also be achieved in the volume of bulk samples using a laser beam focused at a point inside the sample, and then the material remains non-modified on the surface and in subsurface layers.

Obviously, for a stronger display of necessary effects, special materials should be used in such treatments. Easy initiation of processes leading to structural modification of materials is the main property of required layers. The lower is the energy threshold of such modifications in a substance, the easier is the initiation of the process, and the stronger is this effect induced by the treatment. There exist substances in which processes leading to a change of their structure and chemical composition can be activated with an increase of the level of specific energy introduced in unit volume of the substance. Each of such processes is characterised by its own activation energy, and the activation energies of different processes normally differ in value quite widely so that the processes proceed separately. Of course, the more such potential processes can proceed in a material and the lower are the activation energies of the processes, the wider is the diversity of forms and transformations that can be induced in such an initial material.

Metastable germanium monoxide layers can serve such a material. The capability of such layers to transformation into a chemically and structurally stable germanium dioxide allows us to include modifications typical of GeO_2 in a number of possible modifications of initial GeO(solid) layers. During the decomposition of GeO(solid) layers, atomic germanium forms quantum-sized Ge-nanoparticles; this process also adds to the potential of possible transformations.

The two unique properties of film systems based on germanium oxides, their capability to easy modification of their electron and lattice subsystems, are well complemented with a third unique capability – easy transformation of material properties under pulsed laser irradiation. Local laser pulse treatments of the samples were found to be a technique enabling easy modification of germanium oxide layers. This technique offers us a unique tool for realising the potential inherent to germanium oxide layers. Thus, the content of this chapter aims to acquaint the reader with the main results of our investigations in the indicated field.

2. Experimental methods

2.1. Methods of synthesis of GeO(solid) layers and GeO_2<Ge-NCs> heterolayers

The studied films were obtained using three film deposition methods. First, heterolayers of GeO_2<Ge-NCs> were deposited from supersaturated GeO vapour in a low-pressure chemical vapour deposition (LP CVD) process (Knoss, 2008) onto substrates located in a quartz flow reactor (Fig. 1). The implemented LP CVD process involves two stages. The first stage (Fig. 1, zone A) is the formation of germanium monoxide molecules (GeO(gas)) according to the reactions:

$$2Ge(solid) + O_2(gas) \rightarrow 2GeO(gas) \tag{1}$$

$$Ge(solid) + H_2O(gas) \rightarrow GeO(gas) + H_2(gas) \tag{2}$$

The second stage (Fig. 1, zone B) involves two subsequent processes (a and b) proceeding during deposition of supersaturated GeO(gas) onto substrates. Process a is the condensation of vapour molecules (GeO(gas) → GeO(solid)) proceeding with the formation of a homogeneous metastable solid layer of germanium monoxide (GeO(solid)) on the substrate. The solid GeO film is metastable, and it readily decomposes into Ge and GeO_2 (process b) in several minutes at relatively low temperatures about 300°C and over:

$$GeO(solid) \rightarrow ½Ge + ½GeO_2 \tag{3}$$

In reaction (3), the germanium dioxide GeO_2 forms a glassy matrix, with excess germanium atoms being segregated as Ge-nanoparticles. The film growth rate depends on GeO vapour pressure and substrate temperature. In this way, using reactions (1) – (3) we were able to obtain either GeO_2 films with Ge-nanocrystals with sizes ranging from ~ 2 nm to ~ 10 nm (higher deposition temperatures, see Fig. 1 b, area III), or GeO_2 films with amorphous Ge-nanoclusters (lower deposition temperatures, Fig. 1 b, area II), or GeO(solid) films (deposition at room temperature, Fig. 1 b, area I). It should be emphasised here that the heterostructures used in our experiments had the following remarkable property: their molar ratio between Ge and GeO_2 was always fixed at exactly 1:1 independently on particular implemented growth conditions. The surface density of Ge-nanoclusters in a single-layer coating could range from ~10^{10} to ~10^{14} NC/cm^2, the average distance between Ge-nanoclusters being 1/2 of their diameter.

To obtain thin, stoichiometric, nondecomposed and homogenous GeO films on various substrates, a second method was employed. GeO(solid) films were additionally deposited onto substrates using thermal re-evaporation in a high-vacuum (10^{-7} Pa) flow reactor of thick GeO_2<Ge-NC> heterolayers (400–500 nm) grown by the first method (Sheglov, 2008). In such a process, a sample with a GeO_2<Ge-NCs> heterolayer was heated to a temperature of 550–600 ◦C by an ohmic heater. The heated GeO_2<Ge-NCs> film evaporated in accordance with the reverse of the deposition reaction:

$$½GeO_2(solid) + ½Ge(solid) \rightarrow GeO(gas) \quad (4)$$

The resulting GeO vapour condensed onto a cold substrate (T ~ 25 °C), yielding a layer of metastable solid germanium monoxide GeO(solid): GeO(gas) → GeO(solid) (Fig.2). At temperatures T > 250 °C the GeO(solid) films decomposed, according to reaction (3), into Ge and GeO_2 with the formation of a new GeO_2<Ge-NCs> heterolayer.

In the third method (Ardyanian et al., 2006), using evaporation of GeO_2 with an electron beam in a high-vacuum chamber followed by deposition of evaporated species onto substrates at a low temperature (100 °C), we were able to obtain non-decomposed GeO_x films with x = 1,2. Those films, of thicknesses about 300 nm, were obtained in Laboratoire de Physique des Matériaux (LPM), Nancy-Université, CNRS, France. In both cases, with the help of the decomposition of GeO(solid) proceeding according to reaction (3), we could obtain layers of GeO_2 with embedded Ge-nanoclusters.

All studied films were deposited onto either Si (100) substrates or glass. To avoid evaporation of the GeO(solid) films during laser treatments, the samples were covered with protective SiO_2 or SiN_xO_y layers. Protective SiN_xO_y cap layers about 25 nm thick were deposited at 100 °C using the plasma enhanced chemical vapour deposition method (PE CVD), in Institute of Semiconductor Physics of the Siberian Brunch of Russian Academy of Science (ISP SB RAS). Protective SiO_2 cap layers were prepared using two methods. The first method was the evaporation of fused silica glass with an electron beam at 100 °C in a high vacuum (10^{-8} Torr); this method was implemented at Nancy-Université, France (Jambois et al., 2006). The second method was chemical vapour deposition of SiO_2 layers with simultaneous monosilane oxidation in the pressure range 0,5-1,2 Torr at 150°C; this method was developed and implemented at ISP SB RAS.

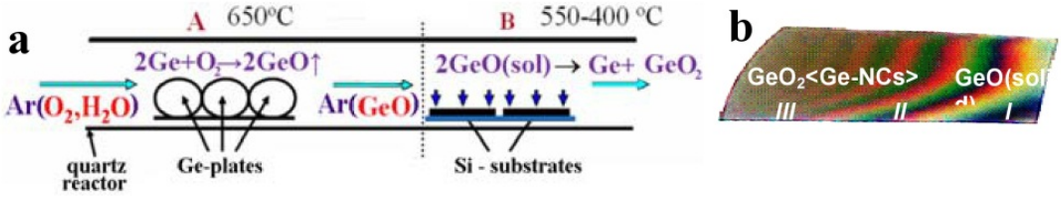

Figure 1. The scheme of LP CVD process of GeO_2<Ge-NCs> heterolayer growth (a); and photo of the GeO_2<Ge-NCs> film on Si-substrate of gradient thickness, structure and features (b).

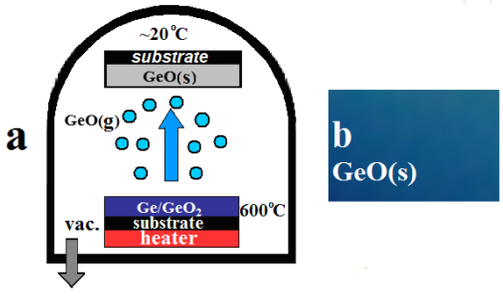

Figure 2. Scheme of vacuum GeO(solid) formation (a); and photo of the GeO(solid) film of uniform properties on Si-substrate (b).

2.2. Methods of structural analysis

Investigation into the structural properties of thin layers of amorphous dielectrics, and also investigation into the impact of various growth factors and technological treatments on those properties, present most challenging problems in modern material science for micro- and nanoelectronics. This usually requires a complex of specific instruments and methods. We examined our films using Raman scattering spectroscopy, IR spectroscopy, ellipsometry, scanning electron microscopy (SEM), transmittance electron microscopy (TEM), and atomic force microscopy (AFM).

The optical constants of our films were studied with the help of the scanning ellipsometry method, implemented with step δl=0,5 mm, using a He-Ne laser (633 nm). The results were interpreted using a specially developed algorithm described elsewhere (Marin et al., 2009). The spectral dependences of absorption and refraction indexes, k(D) and n(D), versus the diameter of Ge-nanoclusters (D) contained in the films were studied using many-angle, multiple-thickness spectral (250-800 nm) scanning ellipsometry. With the combination of spectral many-angle, multiple-thickness measurements, we were able to significantly improve the accuracy of ellipsometric data on the thickness and optical constants of studied films in the visible range.

Atomic force microscopy (Solver P-47H, NT-MDT, Russia) and scanning electron microscopy (Hitachi S4800) were used to examine the surface morphology of our films before and after applied modifications. Optical microscopy was used to register changes in the optical constants of the films in laser-modified areas. The direct observation of Ge-nanoclusters in GeO_2 films was carried out with the help of transmission electron microscopy (TEM) on specially prepared thin SiO_2 membranes (Gorokhov et al., 2006).

Raman spectroscopy was used to reveal and identify the structure (amorphous or crystalline) of Ge-nanoclusters in the films. Raman spectra were registered in quasi back-scattering geometry with a 514,5-nm Ar^+ laser used as an excitation source. A double DFS-52 spectrometer and a triple T64000 Horiba Jobin Yvon spectrometer equipped with a micro-Raman setup were employed. In the latter case, slightly unfocused laser beam was used, producing a spot of about 3-4 micrometer diameter on the surface of the sample, with the laser power reaching the sample being diminished to 10-20 mW in order to avoid overheating of the films. All Raman spectra were measured at room temperature.

IR spectroscopy (FT-801 Fourier spectrometer, ISP SB RAS, Russia, equipped with a micro-setup) was used to study the chemical composition and structure of dielectric layers after different treatments given to them in small areas of the sample. IR absorption measurements carried out at normal incidence were performed at a resolution of 4 cm^{-1}.

Treatments of GeO(solid) layers were performed using a nanosecond KrF excimer laser (wavelength 248 nm, pulse duration 25 ns). Laser fluences ranging from 130 to 170 mJ/cm^2 were applied. A Ti-Sapphire laser (FemtoPower Compact Pro, Femtolasers Produktions GmbH) with 800 nm central wavelength and pulse duration < 30 fs was used for laser treatments. The energy distribution in the laser spot was assumed to have a Gaussian form.

The laser fluence was changed by varying the laser pulse energy E_{pulse}: $E_0 = 2E_{pulse}/\pi r_0^2$, where E_0 is the maximum energy and r_0 is the laser spot radius. The treatments were done in scanning mode with the laser spot diameter being 70 or 1 μm.

3. Peculiarities of GeO(solid) films and GeO_2<Ge-NCs> heterolayers

3.1. The structure and the decomposition process of the metastable GeO(solid) layers

Because of the weak interest of researchers to the films of germanium oxides, nowadays in the scientific literature there are no unambiguous data about the structure of GeO(solid) layers, about the mechanisms of formation of such layers under different conditions, and about their decomposition according to the reaction (3) or evaporation of decomposed GeO(solid) films under heating according to the reaction (4) (Kamata, 2008). However, for controllable variations of the GeO(solid) layers structure and properties, adequate to reality considerations on these aspects are required. This urged us to look for answers to these questions. The qualitative considerations described below are different in that its main statements do not contradict to any fact from known experimental data on GeO(solid) layers. By analogy, one can extend this consideration to the description of the behaviour and properties of SiO(solid) films, since Ge and Si are both group IV elements, this circumstance makes compounds of germanium and silicon with other elements quite similar.

The technology of the films consisting of Si- or Ge-QDs introduced in a dielectric SiO_2 or GeO_2 matrix, respectively, demands understanding of the role and properties of SiO and GeO monoxides. They can be solid and gaseous. However, the physical chemistry of Ge and Si lower oxides is studied insufficient. The actuality of their studies originates from the fact that GeO(gas) condensation in the form of a thin GeO(solid) film is the simplest way of obtaining Ge-QDs dispersed in the glassy GeO_2 film. As the GeO(solid) structure is thermodynamically unstable, the film quickly decomposes due to reaction GeO(solid) → ½Ge + ½GeO_2. To obtain vapour from GeO molecules, one can easy use inverse reaction ½Ge + ½GeO_2 → GeO(gas) at T > 500 ^{0}C (Knoss, 2008). The produced heterolayers with a high Ge-QDs concentration in GeO_2 matrix have the peculiarities which are interesting from both scientific and practical standpoints (Knoss, 2008). For controllable variations of the GeO_2<Ge-NCs> heterolayers structure (in particular, of Ge-nanoparticles characteristics), reliable control of the decomposition process of GeO(solid) layers and a good understanding of the nature of its thermodynamic metastability are required. So we had to look for an explanation to one of the unsolved properties of solid germanium monoxide – thermodynamic metastability of GeO(solid).

In studying germanium monoxide, there arises a question why GeO molecules in gaseous state are stable (dissociation energy ΔH^o ~159 kcal/mole (Jolly & Latimer, 1952)), whereas in solid GeO germanium atoms turn out to be capable of easily breaking their bonds with oxygen atoms without any activation at room temperature. The difference in the stability of the two, gaseous and solid, aggregate states of GeO can be attributed to the fact that the Ge- and O-atoms in a GeO vapour molecule have no immediate interaction with other atoms.

Obviously, sp^3-hybridization (tetrahedral orientation of the four orbitals of Ge-atom) in this molecule is not possible. Therefore in a GeO(gas) molecule the Ge-atom is bonded with the O-atom with one σ-bond and one π-bond (Tananaev & Shpirt et. all, 1967)**.** Transformation of Ge-atom orbitals from sp^3-hybridized state (inherent to solid Ge and GeO_2) into the structure of valence bonds inherent to GeO(gas) molecules requires energy ΔH_{298}~54kcal/mole *(*Jolly & Latimer, 1952*)* and heating.

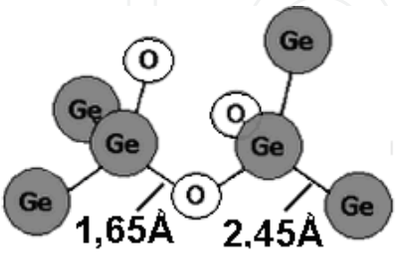

Figure 3. Assumed structure of the atomic network of GeO(solid) satisfying the following two conditions: the valence orbitals of Ge-atoms are ***sp³***-hybridized and the chemical composition of the GeO(solid) film complies with the Ge-O stoichiometry.

When diatomic GeO(gas) molecules condense, the distances between individual GeO molecules become the order of the atomic size. As a result, Ge- and O-atoms become able to be bonded into 3D network from chains of Ge- and O-atoms. The latter allows sp^3-hybridization with tetrahedral orientation of the valence orbitals of Ge-atoms to form the base for construction of an atomic network. The driving force for such a transformation can be the release of free energy spent on the formation of a new valence bond structure of GeO(gas) molecules (reaction (4)). Thus, as the lattices of germanium dioxide and germanium, the lattice GeO(solid) should consist of linked tetrahedra. According to the stoichiometry of GeO each Ge-atom at the vertex of a tetrahedron, formed by its sp^3-hybridized bonds, should be bonded to two other Ge-atoms and two O-atoms (see Fig. 3).

However, there are differences between the lengths of Ge-Ge (2,45 Å) and Ge-O (1,73 Å) bonds in the elemental tetrahedrons of the GeO(solid) lattice. Therefore, this lattice is heavily deformed and has strongly distorted bond angles. So, the real structure of GeO(solid) is not compact, its lattice energy is not minimised to ensure the stability of the atomic network. The latter situation is typical of materials and their basic lattice elements have a low degree of symmetry. When such elements become arranged in a continuous atomic network by successive translations, large cavities should appear in the film. To make such cavities filled with the material, strong deformations of the translation elements, tetrahedrons, become necessary. In any case, the formed atomic network possess a high level of internal strain energy. This will force GeO(solid) to decompose into components, the structure of such components is constructed from (a) basic elements with a higher degree of symmetry and based on sp^3-hybridization of Ge-atom orbitals (b). I.e. these basic elements must provide a layering of unstable material Ge(solid) into the components made without the high internal strain energy. Such components are Ge and GeO_2 which have stable lattices based on elements with high degree of symmetry – $Ge(Ge^{3-})_4$ and $Ge(O^{4-})_4$ tetrahedra, respectively.

A model for the atomic structure of GeO(solid) were developed on data received by IR and Raman spectroscopy, scanning probe microscopy and new methods in high-resolution TEM and ellipsometry. The model allows us to consciously control the structure of heterolayers GeO_2<Ge-NCs> during their growth and further treatment. An analysis of structural transformations of germanium monoxide based on this model allows gaining a better insight into some important details of the formation of the metastable GeO(solid) atomic network during condensation of GeO(gas) molecules and of decomposition under activating treatments. According to the above model, the formation of stable GeO_2<Ge-NCs> heterolayers proceeds in two steps. The first step is the formation of a homogeneous metastable GeO(solid) structure at T< 100-200^{o}C, when GeO(gas) molecules condense from vapour onto the surface of the growing GeO(solid) film. It is a very rapid process (femtoseconds) proceeding when the atomic bonds of Ge- and O-atoms in absorbed GeO(gas) molecules get rearranged into tetrahedral configuration of sp^3-hybridized bonds; the process has a very high rate and the duration of this process is defined by the switching time of valence bonds between chemically interacting atoms.

Note that if during the condensation of GeO(gas) molecules its diatomic molecules cannot approach each other at atomic distances, the structure of the valence bonds of those molecules remains unaltered. It follows from the data by Ogden and Ricks (Ogden & Ricks, 1970), who found that during condensation GeO(gas) molecules readily become incorporated into the solid matrix of frozen N_2 or Ar at T ~ 20 K. Under such conditions, the vibrational spectra of GeO(gas) molecules (Fig. 4 a) show no changes during freezing in the solid state, and their IR absorption spectra are no difference from the spectra of GeO vapour molecules. In contrast, in the case of condensation of GeO(gas) molecules proceeding with the formation of a GeO(solid) film, vibrational characteristics of the atomic network change considerably (see Fig. 4 b). IR spectrum of frozen GeO molecules has no band, which is typical for GeO(solid) during its thermal decomposition in the range of 770 - 870 cm^{-1}.

The second step is a process of rearrangement of the homogeneous but metastable lattice of GeO(solid) layer into a complicated heterogeneous film structure such as a solid glassy GeO_2 matrix with incorporated Ge-nanoparticles. The latter process is more difficult and by order of magnitude slower than the former process. At this step, two stages can be marked out. The first stage involves decomposition of the lattice of the GeO(solid) layer, with half of the Ge-atoms of this lattice becoming bonded to the bridge O-atoms with all the four sp^3-hybridized bonds of each Ge-atom. Here, a solid GeO_2 network made by $Ge(O^{2-})_4$-type tetrahedrons forms. This network fills up the volume that was previously fully occupied by the 3D GeO(solid) network. On the contrary, the second half of the Ge-atoms in the decaying GeO(solid) network tends to fully disrupt its sp^3-hybridized valence bonds with O atoms to get out of the atomic network of solid germanium oxide. However, because of the impossibility to do that immediately, these atoms are forced to form various defects in glassy GeO_2. The variety of atomic configurations in GeO_2 layers could be rather large. But the numerous atomic configurations can be subdivided into two fundamentally different types: type 1 is Ge-atoms at interstitial sites not bonded to the lattice; and type 2 is Ge-atoms partially preserving their bonds with the lattice. In the latter case, such atoms are elements

of sp^3-hybridized distorted tetrahedra involved in continuous chains formed by undistorted, successively aligned tetrahedra. The distorted tetrahedra are tetrahedra lacking some bridge O-atoms on their tops; i.e. the central Ge-atom of such a tetrahedron has one to three dangling sp^3-hybridized valence bonds or those bonds link the central Ge-atom to other Ge-atoms (here, different combinations of the two variants are also possible). Note that during the formation of the GeO_2 network from the lattice of GeO(solid), there is no need in a transfer of large masses of substance between remote sites in the volume of the material. Structural rearrangements of the 3D matrix proceed simultaneously in a huge number of centres, and the rearrangement processes proceed in a local vicinity of each centre.

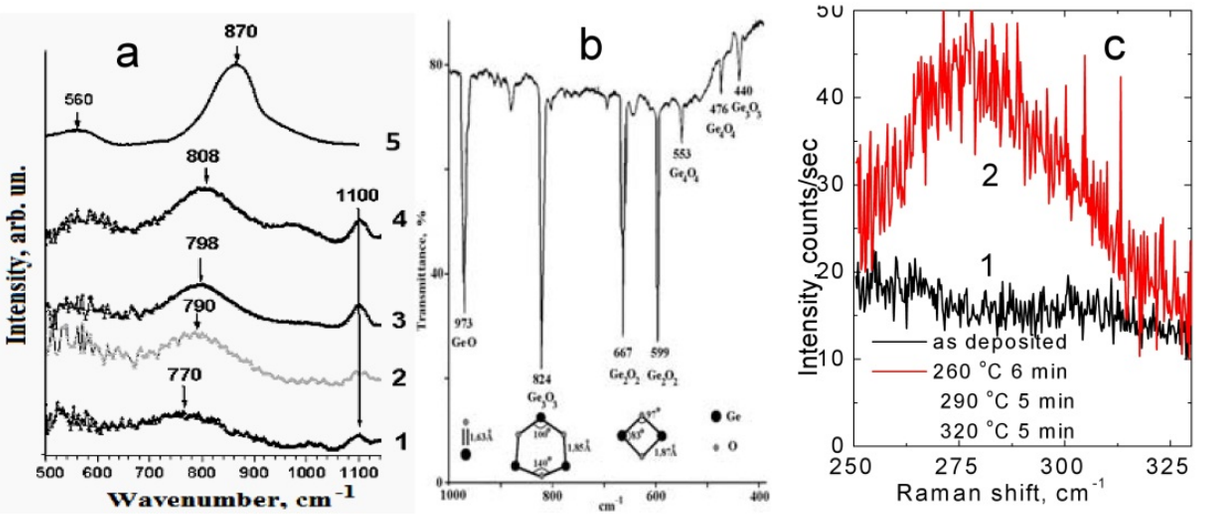

Figure 4. a - IR transmission spectra of gaseous GeO molecules (monomer, dimer, trimer, tetramer), embedded in matrix of frozen N_2 or Ar at T = 20 K (Ogden & Ricks, 1970); b - IR absorption spectrum of GeO(solid), prepared by condensation of GeO vapour: **1** - as-deposited; **2, 3, 4, 5 -** annealed at 260ºC/6 min; 290ºC/5 min; 320ºC/5 min; 600ºC/10 min, respectively; c - Raman spectra of GeO(solid): **1**- as deposited; **2** – after series of annealings at 260ºC/6 min; 290ºC/5 min; 320ºC/5 min.

That is why migrations of many atoms turn out to be quite localised processes. However, simultaneous decay of one lattice and formation of the other lattice lead to the formation of a multitude of various defects in the forming atomic network. The density of such defects is several orders higher than the values typical of the equilibrium lattice states. As a result, simultaneously with the intensive formation of defects in the GeO_2 network, there may be no less intensive annihilation of such defects and complementary defects. Hence, during structural rearrangement of a GeO(solid) film into a heterostructure, density and viscosity of the material should considerably decrease. Of course, the characteristic times of such rearrangements must be large and depend on the temperature and other external factors. The structural modification process of germanium oxide lattice in the initial GeO(solid) layer subjected to successive anneals is shown in IR spectroscopy data (Fig. 4 b). Film of 55 nm thickness was deposited at T~ 25 °C. After two annealings (260 and 290 °C) shrinkage of

layer thickness occurred by ~ 6-8% according to ellisometric data, as a result the structure of discussed heterosystem seeks to optimise its stable parameters: the size, the number of defects in the atomic net, the excess of internal energy, etc.

The above specific features of the rearranging lattice of the oxide layer facilitate the nucleation of Ge-nanoclusters in the volume of the GeO_2 matrix, the second component of the structural arrangement process of GeO_2<Ge-NCs> heterolayer. Very likely, this process is the slowest one among the above-discussed processes, as Ge-atoms need to lose their continuous bonds with the oxide lattice and, then, migrate over sufficiently large distances (much larger than the size of the "unit cell" in the oxide network) to enter the structure of growing Ge-clusters. The segregation kinetics of amorphous germanium in GeO(solid) layers annealed at different temperatures is reflected in the Raman data shown in Fig. 4 c. Combined Raman spectroscopy and HRTEM data show that germanium initially forms small amorphous Ge-particles sized several nanometers; on increasing the temperature and the duration of the film synthesis process and subsequent anneals, those particles grow in size to form larger Ge-particles sized several ten nanometers. According to Raman data, at T ~ 470-490 ^{0}C, amorphous Ge-particles undergo crystallisation. At T > 600^{0}C, in a GeO_2<Ge-NCs> heterostructure the GeO_2 matrix may also transform into hexagonal phase, which is isomorphous to α-quartz (Gorokhov, 2005).

3.2. Elementary GeO_2 lattice defects in modifications of GeO_2<Ge-NCs> heterolayers

Analysis of rearrangement processes proceeding during decay of metastable germanium monoxide layers should be performed considering the fact that such processes are controlled by regularities typical of glasses rather than crystals, as microscopic mechanisms underlying lattice transformation and relaxation processes in glasses and crystals are radically different. For gaining a better insight into substance modification processes proceeding in GeO_2<Ge-NCs> heterosystems under pulsed laser treatments, we have to first consider the role of elementary defects in glass atomic network during its formation and subsequent treatments.

In glasses transitions during melting and freezing do not have a sharp boundary. Such processes proceed gradually as the glass viscosity (η) continuously decreases (upon heating) or increases (upon cooling). Vitrification temperature (T_g), at which glass viscosity $\eta=10^{13}$ P, is accepted as the phase transition point. At $T < T_g$ glassy materials are solid, with the majority of atomic bonds in their bulk being not broken; at $T >> T_g$ the materials are melted, with their atomic bonds undergoing rupture, and that provides the material's easy flow ability. Silicon and germanium oxides are basic natural glass-forming materials, but the vitrification temperatures of pure SiO_2 and GeO_2 are strongly different ($T_g(GeO_2)$ =570^{0}C, $T_g(SiO_2)$ =1170^{0}C), causing a considerable difference in material properties of silicate and germanate glasses. However, the physicochemical mechanisms underlying the behavior and properties of silicate and germanate glasses and the mechanisms controlling structural and chemical modifications of the two groups of glasses, do not have vital differences, although

quantitative characteristics defining material properties and processes in glasses are usually considerably different.

The viscous glass flow is a thermally activated process: $\eta(T)=A\cdot exp(Q/RT)$, where Q is the viscosity activation energy and A is a constant. In amorphous materials, the viscous flow clearly deviates from the Arrhenius law: in such materials, the viscosity activation energy Q changes its magnitude from a higher value Q_H at low temperatures (glass state) down to a smaller value Q_L at high temperatures (liquid state). In the theory of glass viscosity (SiO_2, GeO_2 and others), much attention is normally paid to defect migration in the glass atomic network. Presently available models of this phenomenon are based on the Mueller hypothesis (Mueller, 1955, 1960) about switch-over of oxygen bridge bonds in material. According to this hypothesis, during viscous melt flow, covalent Si-O (or Ge-O in GeO_2 glass) bonds do not break (Appen, 1974), but they switch over (translate, reorient). That is why the mechanism of viscous flow in mechanically loaded materials consists of two different stages, preliminary local re-grouping of valent bonds due to thermal fluctuations and switch-over of oxygen bridge bonds. At first stage, low-activated glass network extension proceed. Due to thermal fluctuations, basic structural elements (SiO^4 tetrahedrons) undergo deformation and regrouping of their valent Si-O bonds, i.e. the bond angles slightly change their values and atoms in Si-O-Si bridges become displaced from their previous positions. As the interaction between covalent atoms is short-range and oriented, the pair interaction energy sharply increases at large changes of interatomic distance. The activation energy of atom regrouping proceeding without chemical bond rupture is close to the mean thermal motion energy of atoms in glass melt; and, according to estimates, 100-150 atoms should participate in formation of microvoids of the required size (Nemilov, 1978). Such local fluctuations of valent bond configurations are necessary for subsequent elementary kinetic acts, namely switch-over of oxygen bond in Si-O-Si bridges (Filipovich, 1978; Mueller, 1955, 1960). Here, one of the oxygen bonds with silicon atoms undergoes disruption, and it switches over to another Si-atom having a vacant bond (Fig. 5). As a result of the rearrangement process, the O-atom shifts at one interatomic distance, and that is possible due to the presence of a microvoid earlier formed in the vicinity of the O-atom. Such bonds switches over occur in crystals during dislocations glides in the time of plastic flow.

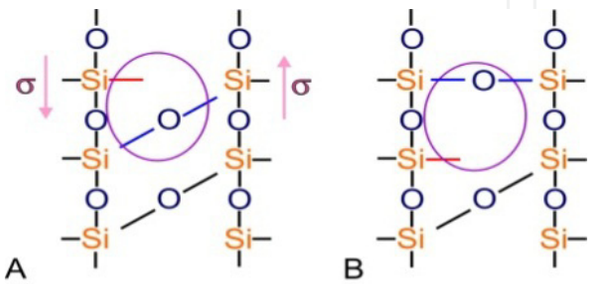

Figure 5. Mechanism of viscous flow in SiO_2 (or GeO_2) glass proceeding as a result of silicon vacant bond switching in Si-O-Si bridges: A - initial state; B - after Si vacant bond switching

The activation energy of the bridge oxygen switch-over is a sum of two components. The first component is the relatively low microvoid formation energy, or fluctuating local silicon-oxygen network deformation energy ~4 - 5 kcal/mol (Sanditov, 1976). Herein, the energy barrier of the second process, direct switch-over of bridge oxygen bonds, decreases to some minimal level of ~20 - 30 kcal/mol, which is different for various glasses. However, if a small number of atoms (3 - 4) participate in the bridge oxygen bond switch-over process, up to ~100-150 atoms are involved in the local deformation of the silicon-oxygen bulk. The latter circumstance provides for a substantial contribution of the entropy term to the effective glass viscosity activation energy, H^*_η. Vacant bonds switch-over activation energy in the glass viscosity theory is connected with formation mechanism of bonds (Filipovich, 1978; Nemilov, 1978; Sanditov, 1976; Zakis, 1981; Mueller, 1955, 1960; Nemilov, 1978), i.e. with a predominant way of vacant bonds formation and switch-over type. However, rather low activation energies of ~25-35 kcal/mol and large pre-exponent multipliers are typical of the temperature dependencies of bond switch-over rates, providing for most defects migration in the glass network and for the viscous flow of glass at $T \sim T_g$. Therefore, the processes conditioned by directed bonds switch-over (viscous flow, crystallisation, chemical interaction, and diffusion) proceed, as a rule, at relatively low rates, which is typical of the chemical properties of polymeric glass-forming substances (Appen, 1974).

All the above regularities suggest that, in GeO_2<Ge-NCs> heterolayers, oxygen vacancies generated in glassy GeO_2 matrix at T > 500^0C (i.e. at temperatures close to $T_g(GeO_2)$) at the boundary of Ge-nanoparticles can easy move within matrix volume. Translation of bridge oxygen bonds to vacant bonds of Ge-atoms underlies migration of oxygen vacancies. Maximum values of equilibrium vacancies concentrations in GeO_2 glass are high; as a result, this mechanism becomes capable of providing mass transfer of Ge-atoms through oxide in the heterolayer towards the boundaries of Ge-nanoclusters. In this way this mechanism contributes to Ge-nanoclusters growth. During decay of GeO(solid) atomic network at temperatures over ~250 °C, the decomposition process of this network, leading to releasing of half the total amount of Ge-atoms initially contained in GeO(solid), ensures excessive supply of vacant oxygen bonds towards the forming GeO_2 matrix. The rearrangement of valence bonds of Ge-atoms in the sp^3-hybridization form is accompanied by the release of considerable energy. During rearrangement, the switch-over of bridge oxygen bonds to vacant bonds requires the least energy in comparison with all other potential barriers. For a number of glasses, the activation energy of the switch-over falls in the range from 23 to 37 kcal/mol, these values are close to the activation energy of oxygen atoms hops in alkaline-silicate glasses (Gorokhov, 2005).

3.3. Densification of GeO_2<Ge-NCs> heterolayers and them moisture absorption

The majority of physical and chemical processes in the modification of lattices in GeO(solid) and GeO_2 layers should be analysed in terms of structural rearrangements with active participation of oxygen vacancies. First of all, such processes include densification of heat-treated layers and adsorption/desorption of moisture from atmosphere in the material.

The densification process is due to the fact that the high rate of GeO molecules condensation from vapour at low temperatures (< 200-250 °C) forms low-density GeO(solid) layers with high concentration of lattice defects. Concentrations of various point defects and their ensembles, pores and other microvoids in the film lattice are much higher than the values typical for the quasi-equilibrium state of atomic network. Such a structure is typical of CVD SiO_2 layers, especially deposited at T < 500 °C. This structure has a zeolite-like behaviour, which disappears completely after annealing at T > 700 °C and is manifested in the ability of CVD SiO_2 films during the storing to absorb in their volume water molecules and other atmospheric vapours. The absorbed moisture fills all kinds of defects in the volume of the film atomic network. Besides, part of H_2O molecules absorbed in the film dissociates into hydroxyl groups OH^- and hydrogen ions H^+ fix at vacant bonds of atoms in the oxide lattice.

Annealing of CVD SiO_2, GeO(solid) and GeO_2 layers at temperatures over 250-300 °C activates processes leading to a decrease of nonequilibrium defects concentration in the atomic lattices of the oxides. Usually this leads to an increase of film density with simultaneous decrease of film volume (shrinkage), as well as to increased optical constants, decreased conductivity, increased tensile stress and viscosity of the material. The intensity of the process and the degree of film properties change depend on the temperature, anneal duration and atmosphere in which anneals were held, as well as on the defects density (or imperfection) of the initial atomic network of the film. Typically, the stronger the thermal treatment and more defective the films, the higher the degree of change of basic film characteristics. For instance, the shrinkage degree in thickness of CVD SiO_2 and Si_xN_y(H) films varies within the range from 3-5 to 25-30% (Gorokhov et al., 1982; Pliskin et al., 1965). The presence of absorbed moisture in the film increases its ability to shrink. Therefore, protective (cap) layers are used for protection of GeO(solid) and GeO_2 layers from the degrading effects of atmosphere. Thin (tens of nm) low-temperature PE Si_xN_y(H) films are the best encapsulating coatings. The protection ability of CVD SiO_2 layers is worse, so one should increase their thickness. Note that during anneals moisture leaves the GeO(solid) and GeO_2 layers faster than CVD SiO_2 layers. Anneals at 150-180 °C during ~ 30-40 min in vacuum or in a flow of a pure and dry inert gas are sufficient for effective moisture desorption from germanium oxide layer 150-200 nm thickness.

3.4. Other methods of structure modification of GeO_2<Ge-NCs> heterolayers

The composition and structure of GeO_2<Ge-NCs> heterolayers can be easily modified chemically. Removal of the glassy GeO_2 matrix from GeO_2<Ge-NCs> heterolayer is the simplest way. Glassy GeO_2 is readily soluble in water and, especially, in aqueous solutions of HF, whereas crystalline or amorphous Ge-nanoparticles remain unaffected by such solutions. On dissolution of GeO_2 matrix, Ge-nanoclusters initially contained in the volume of a GeO_2<Ge-NCs> heterolayer agglomerate with each other due to very weak electrostatic forces and settle on the substrate forming a weakly coupled, very loose and porous Ge-layer. So, very thin GeO_2<Ge-NCs> heterolayers can be used to produce, for example, single-layer coatings formed by Ge-nanoparticles on substrates of different materials. An annealed

agglomerative layer of Ge-nanoparticles becomes sintered, and a more durable Ge-coating with a porous structure forms. Such a layer was formed inside a multilayer structure containing SiO_2 films in order to examine the effect of femtosecond (fs) laser treatments on this layer (see Fig. 6 a). Under ablation, after the explosive action of fs laser pulses a region of porous germanium was detached from the thick SiO_2 layer, turned over and thrown away onto the undestroyed part of the multilayer system. As a result, we became able to obtain a SEM image of the upper and lower surfaces of the layer under study (see Fig. 6 b).

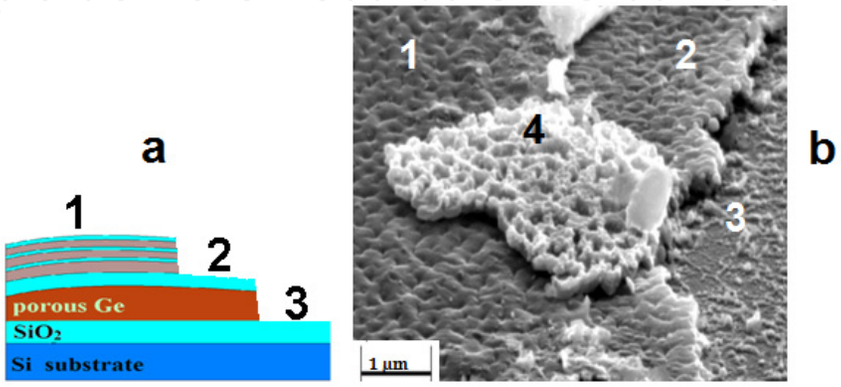

Figure 6. Surface morphology of a multilayer coating after fs laser treatment : **a** - scheme of coating structure consisting of three tiers: the bottom tier is Si-substrate with the first SiO_2 film (of 100 nm thick), middle tier is a Ge-porous layer (of ~ 70-230 nm thick) coated by second SiO_2 film (of 100 nm thick), and upper level is three bilayer structures, each of them consists of thin heterolayer GeO_2<Ge-NCs> (of ~ 15 -25 nm thick) coated by the SiO_2 cap-layer (of 10 nm thick) (CVD SiO_2 is shown as blue, Ge-porous and GeO_2<Ge-NCs> layers – as brown); **b** - SEM image of the multilayer coating surface: **1** – unmodified by radiation, **2** – after liftoff of the top tier; **3** - surface of the lower SiO_2 layer after liftoff of the Ge-porous layer; **4** - surface morphology of the back side of the Ge-porous layer fragment produced by laser damage.

Processes of oxidation and shrinkage of GeO(solid) layers and GeO_2<Ge-NCs> heterolayers are similar. We found that oxidation of GeO_2<Ge-NCs> heterolayers in an oxygen flow at normal pressure differs little from the oxidation of pure germanium wafers under the same conditions. The process can be well monitored ellipsometrically at temperatures over ~500^0C. Under such conditions, GeO(solid) layers disproportionate into Ge and GeO_2 according to reaction (3) for a time not longer than 2-3 minutes, and then they undergo oxidation as GeO_2<Ge-NCs> heterolayers. Ge-nanoparticles oxidation front propagates from the surface of the film into depth. The kinetics is close to kinetics of pure germanium oxidation even quantitatively. The mechanism of the process is that the Ge/GeO_2 interface in the system generates vacant bonds ("oxygen semi-vacancies") on Ge-atoms incorporated in the formed oxide network. Further on, these vacant bonds tend to maximally fill the GeO_2 lattice by their translation mechanism. O-atoms from the molecules of ambient O_2 get captured by vacancies on the exposed external surface of the oxide layer. After this captured O-atom becomes attached with one of its bonds to the GeO_2 network while the other bond usually remains free. In the oxide this free bond presents one quarter of a Ge-atom vacancy

and is excessive (non-equilibrium). Thus, the interdiffusion of oxygen semi-vacancies and quarters of germanium vacancies in the oxide layer network, accompanied by gradual annihilation of these complementary defects, is the oxidation process of both germanium wafers and Ge-nanoparticles in the glassy GeO_2 layer.

Crystallisation of the glassy GeO_2 matrix in GeO_2<Ge-NCs> heterolayers is an exceptionally structural (not chemical) process. We have studied this process using layers of pure thermal germanium oxide on Ge(111) substrates. The most important is that GeO_2 layers begin to rearrange into the low-quartz structure already at 600-620 ^oC; it is worth noting that there are conditions for forming large-area continuous block-epitaxial coatings from crystallised hex-GeO_2 over quite a large area. Interestingly, an analogous process also proceeds in thermal silicon oxide with formation of block-epitaxial β-crystabalite SiO_2 layers. But the latter process proceeds very slowly even at temperatures $T > 1200^0C$. It makes the material practically unpromising in the silicon integral planar technology. Unlike SiO_2, low-quartz GeO_2 layers are more suitable for application, as crystallisation of glassy GeO_2 layers considerably increases the mechanical strength and chemical stability of the films. For removing crystallised layers, etching solutions with considerable HF acid proportion are necessary. It is described in the monography (Knoss, 2008) where reactions of glassy GeO_2 layers with CVD SiO_2 and Si_3N_4 films deposited onto such layers were also described.

Interaction of thermal GeO_2 layers with ammonia at ~ 700-750^0C according to reaction $3GeO_2 + 4NH_3 \rightarrow Ge_3N_4 + 6H_2O\uparrow$ proceeds in the oxide lattice in compliance with the micromechanisms similar to those involved in germanium oxidation (Gorokhov, 2005). At these temperatures the solid reaction product, Ge_3N_4, dissolves in the practically liquid oxide layer and forms a glassy GeO_2:Ge_3N_4 (m:n) layer. Under the described conditions, germanium (both the wafer material and Ge-nanoparticles) also reacts with NH_3 and forms Ge_3N_4. Therefore, relatively thin GeO_2<Ge-NCs> heterolayers can be used to increase the Ge_3N_4 content of the formed GeO_2:Ge_3N_4 glassy layers.

The above reactions are interesting because they allow a drastic modification of the structure and composition of the GeO_2 matrix in GeO_2<Ge-NCs> heterolayers up to ~100 nm thickness. Low viscosity of glassy GeO_2 at temperatures T>Tg provides for rapid mutual solution of SiO_2 layers with germanium dioxide, practically to a homogeneous composition at thickness amounting to hundreds of nanometers; this process transforms the layers into germanium-silicate glass. Varying the thickness ratio of GeO_2/SiO_2 double-layers we can change the composition of composite GeO_2:SiO_2 glass in a wide range of values.

Glassy GeO_2 reacts with CVD Si_3N_4 films at the interface at $T > 700^0C$ according to the formula $3GeO_2 + 2Si_3N_4 \rightarrow 2Ge_3N_4 + 3SiO_2$. Like SiO_2, the low viscosity of glassy GeO_2 alleviates the interdiffusion of initial and final products of this reaction across the interface of the reacting layers. As a result, a layer of glassy GeO_2:Ge_3N_4:SiO_2-type compound several tens-hundreds of nm thickness forms at the interface. The composition of this layer depends on the thickness ratio of initial layers, and on the temperature and duration of the reaction. Under heating held at temperature T ~750^0C for an hour, in the obtained germanium-silicate glass and multi-component GeO_2:Ge_3N_4:SiO_2 → k:p:q layers

crystallisation begins, proceeding similar to that in pure glassy GeO_2. The crystal lattices of the glasses are isomorphic to the low-quartz structure, and they excel hex-GeO_2 layers in chemical stability.

Interestingly, the dramatic increase of density and chemical stability in composite glassy GeO_2:SiO_2 and GeO_2:SiO_2:Ge_3N_4 – k:p:q layers begins already at their formation stage. With the example of GeO_2:SiO_2, it is seen that this effect is much more pronounced in comparison with the effect due to mere linear growth of the more chemically stable SiO_2 fraction in the two-component composition. In other words, the etching rate of the glassy GeO_2:SiO_2 layer in a structurally sensitive etchant turns out to be a few times lower than the individual etching rates of glassy GeO_2 and SiO_2 layers (even when the fraction of SiO_2 in the composition is not high). We suppose this effect been due to the fact that the formation of glassy GeO_2:SiO_2 and GeO_2:Ge_3N_4:SiO_2 – k:p:q films occurs in the vicinity of the crystallisation temperatures of these substances. Therefore, during annealing such glasses should undergo the stage preceding crystallisation. At this stage, the glass atomic network is getting ready to transform into a high-ordered crystal lattice so that the density of quasi-equilibrium defects rapidly decreases. Crystallised glass is known to have lattice defect concentrations orders lower than the initial concentrations of the same defects at the initial stage. Hence, introduction of GeO_2 into glassy SiO_2 provides for a sharp decrease of vitrification and crystallisation temperatures of the composition, together with a sharp decrease of vacancy concentration. Thus, CVD SiO_2 layers with reduced density, due to a high concentration of non-equilibrium defects in rather unstable atomic network, can be etched in etchant sensitive to their structure tens of times faster than quasi-equilibrium thermal SiO_2 layers formed at temperatures ~ 1000 ^{0}C (Pliskin and Lehman, 1965).

Thus, the described structural-chemical modification processes of glassy oxide GeO(solid), GeO_2 layers and GeO_2<Ge-NCs> heterolayers have a high modification ability, which allows us to obtain chemically stable coatings with an original stable structure and chemical composition, high mechanical strength and easily controlled physical, electrical and optical properties from chemically unstable, structurally imperfect, physically and mechanically soft, and electrically unstable layered films.

4. Laser treatments of GeO_2<Ge-NCs> heterolayers

Thermal anneals, traditionally used in microelectronics, were the tool for the described modifications of the composition and structure of the films under study, in which different Ge oxide layers played the main role. As it was noted in Introduction, pulsed laser irradiations offer a considerable resource for enlarging the list of possible chemical and structural transformations can be implemented in the materials of interest. Irradiation of film systems with electromagnetic radiation can be considered as a basic kind of possible treatments. Unlike common thermal treatments, irradiation of samples with light pulses allows a radical widening of the range of conditions that can be realized in the high-energy treatment of layered materials. First, here we mean the value of the energy input in

irradiated materials, which can be orders higher than the limits that can be reached in ordinary heat treatments of samples. Second, the range of dynamic parameters of high-energy effects in irradiated films can also be widened by many orders, together with the spatial localization parameters of such effects. Due to these factors, irradiation of samples with short laser pulses considerably extends the spectrum of possible modifications of thin films in micro- and nanoelectronic structures.

Over more than thirty years, Pulsed laser Annealing (PLA) has been successfully used to achieve crystallisation and re-crystallisation of semiconductor materials in thin-film structures (Dvurechenskiy et al., 1982). Earlier, PLA treatments of thin-film structures with light quanta exceeding in energy the bandgap width of semiconductor material were recognized as a useful means for rapid (typically, during some tens of nanoseconds or less) restoration of the crystalline structure in disordered or even completely amorphized near-surface layers of Si (Ahmanov et al., 1985). At a proper choice of laser parameters, almost all laser radiation can be absorbed within the film; hence, this radiation does not reach the wafer and does not heat it. As a result, short laser pulses allow one to avoid overheating of the substrate during film cooling due to diffusion of heat into the substrate (tens of nanoseconds). That is why PLAs can be used to crystallize amorphous silicon films on substrates not withstanding high temperatures.

Powerful laser impacts lead to fast, high-quality re-crystallisation of amorphized near-surface semiconductor layers. Despite the fact that PLA has already become a well mastered technique, laser annealing experiments raised a number of still unsolved fundamental physical questions (Chong et. al., 2010). Recent contributions have shown that fast laser-induced phase transformations in near-surface semiconductor layers, such as melting-hardening, phase transitions 'amorphous solid – crystal' and 'crystal – amorphous solid', etc., proceed over nano-, pico-, and even subpicosecond time scale. To explain the various and, in many respects, unexpected phenomena observed during PLA treatments of semiconductor structures, it is necessary to give an answer to a number of fundamental questions regarding the behavior of semiconductors in strong laser fields.

PLA is widely used to eliminate structural imperfections and radiation defects introduced during implantation of ions in the near-surface crystal layers (Kachurin et al., 1975). PLAs provide an important possibility for the technology, obtaining perfect crystal structures in subsurface layers with impurity concentrations unreachable in the common thermal annealing (to 10^{21} cm^{-3} and higher). Diffusion of impurities is highly suppressed under PLA conditions (Kachurin et al., 1975). In addition, PLA allows realization of processes that do not occur during common thermal treatments. Such processes, which are of physical concern, are conditioned by the presence of dense plasma in the samples. The range of observed PLA-induced processes includes softening of phonon modes with increasing plasma density, change of bandgap width with increasing n_c (non-equilibrium carrier concentration), registration of optical and electrical phenomena in semiconductors depending on n_c (Ahmanov et al., 1985), etc. Spatial coherence of laser radiation used for pulse laser treatments of semiconductor materials allows creation on the surface of annealed

samples of periodic spatial structures, e.g. lattices formed by alternating crystalline and amorphous regions (the so-called interference laser annealing).

Later, nanosecond pulsed treatments using excimer XeCl (λ = 308 nm) (Volodin et al., 1998) and ArF laser radiation (λ = 193 nm) were used to obtain silicon nanoclusters and achieve crystallisation of a-Si inclusions in SiN_x and SiO_x films (Rochet et al., 1988). Some of the unusual properties of such heterolayers were manifested in samples treated with ultrashort pulsed fs laser radiation (Korchagina et al., 2012). Reports on laser treatments performed to modify the structure, chemical composition, and properties of GeO(solid) and GeO_2 films, and also to achieve formation of c-Ge nanoparticles and crystallisation of a-Ge inclusions in dielectric matrices are encountered much more rarely (Gorokhov et al., 2011).

4.1. Peculiarities of conventional nanosecond PLA

Considering the complexities of PLA impact mechanisms on thin-film semiconductor structures and a complex nature of physicochemistry and structure of glassy GeO(solid), GeO_x, and GeO_2 films, and GeO_2<Ge-NCs> heterolayers, unusual effects could be expected in our films during PLA treatments. Two lasers with different photon energies and durations of light pulses, a KrF excimer laser (wavelength λ = 248 nm, pulse duration 25 ns) and a Ti-Sapphire laser (central wavelength λ = 800 nm, pulse duration < 30 fs), were used in this investigation. As expected, the impacts of short-pulse treatments on our samples for the two lasers turned out different.

The effect of ns radiation was studied for two bilayer systems, GeOx/SiO_2 and Si/GeO_2<Ge-NCs>/SiN_xO_y, both prepared on Si(100) substrates (SiO_2 films of thickness 100 nm and SiN_xO_y films of thickness 25 nm were the cap layers). A sketch of the second system is presented in Fig. 7 a, b. The laser beam was focused, through a square-section diaphragm (200 x 200 μm), on the sample surface. Laser pulses followed at a frequency of 100 Hz, and the beam moved along one of the sides of the square on the sample in ~180-μm increments. After exposure of one band on the sample surface to the beam with a set laser pulse energy (see Fig. 7 d) the beam was shifted a step further to treat the next band under the first one. An exposed film section was formed out of several bands. Because of overlapping of laser spots, the film was exposed to the laser beam two times on the edges of the square and four times in the corners (Fig. 7 c, d and e). Such neighborhood of film regions exposed to different numbers of identical laser pulses (1, 2 and 4) allowed us to trace the pulse-by-pulse changes induced in the regions where the film system acquired different thicknesses.

In the absence of cap layers, the used PLA completely "evaporated" the germanium oxide layers on our samples transforming them into GeO(gas) according to reaction (4). The SiO_2 and SiN_xO_y cap layers, impeding the removal of GeO(gas) molecules, substantially slowed down the formation reaction of those molecules in the protected films. Nonetheless, even in the presence of cap layers the irradiated regions exhibited a notable change in interference colors (Fig. 7 b, c, d, e).

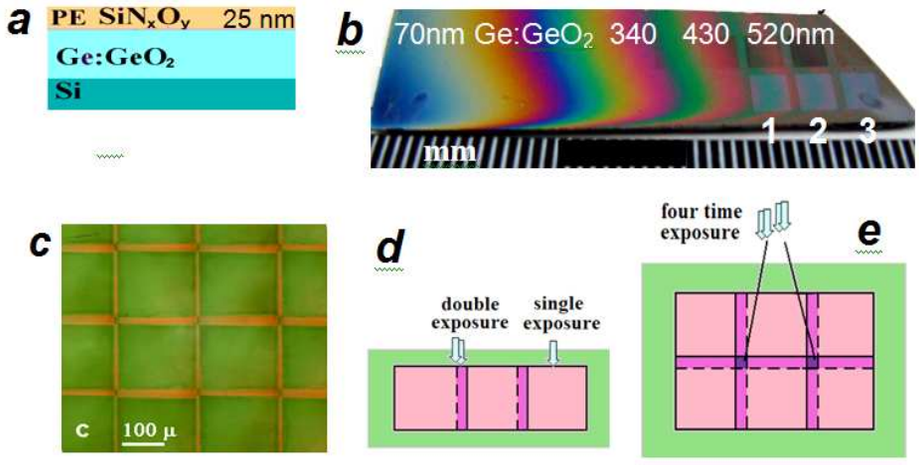

Figure 7. **a** – schematic representation and **b** - photo of the Si/GeO_2<Ge-NCs>/SiN_xO_y bilayer system on Si substrate irradiated with laser radiation to fluences 170, 150 and 130 mJ/cm² in regions 1, 2 and 3 of the heterolayer (thicknesses ~390, ~480 and ~520 nm, respectively); **c** - micrograph and **d, e** – schematic illustrating the formation of single-, double- and four-time exposed areas of the film at stepped irradiation.

4.1.1. Shrinkage of GeO_2<Ge-NCs>/SiN_xO_y bilayer coatings under ns PLA

Data obtained with a set of experimentaltechniques in irradiated regions 1, 2 and 3 of the sample with ~390-, ~480- and ~520-nm thick heterolayers provided a comparison of the type and degree of changes in the structure and material properties of examined films after their exposure to different laser fluences, 130, 150, and 170 mJ/cm². Changes of interference colors in the bilayer system occurred due to strong shrinkage of the materials forming in the system individual layers, which was usually accompanied by increase of film optical constants. The effect here is similar to the one which was studied by ellipsometry and which proceeded with a change of optical constants of GeO(solid) layers during thermal anneals. In the latter case, GeO(solid) did not evaporate because of low annealing temperature. Results of ellipsometric measurements of our samples performed following their thermal treatments in vacuum are shown in Fig. 8. The measurements were carried out using a special method that combined spectral and scanning ellipsometry with multi-thickness measurements (Marin et al., 2009) and that allowed us to obtain sufficiently precise data on optical constants of annealed GeO_2<Ge-NCs> heterolayers throughout the whole visible range of the spectrum.

The data for $k(\lambda)$ (curves 1 - 4 in Fig. 8) show the changes in the bandgap of as-deposited GeO(solid) films and GeO(solid) films given traditional anneals at different temperatures. These changes are the result of the chemical decomposition of film material connected with the appearance in the film and subsequent growth of Ge nanoparticles in which, due 3D

confinement effects, the efficient band gap value decreases with an increase of nanoparticle size, tending at large nanoparticle sizes to the bandgap value of bulk α-Ge. The $k(\lambda)$ data for all examined films were plotted in the Tauc coordinates, with the square root of absorbance coefficient $\boldsymbol{\alpha}$ being plotted along the vertical axis. This coefficient was obtained from the extinction coefficient by formula $\alpha_j(E)=2\pi k_j(E)/\lambda$; here, the parameter j is the number of a studied film in Fig. 8. Using the well-known formula for the absorption coefficient of indirect-band semiconductors, $\boldsymbol{\alpha}^{1/2} \sim (E - E_g)$, and interpolation of the linear dependences of $\boldsymbol{\alpha}^{1/2}$ $(E- E_g)$ to $(E- E_g) \rightarrow 0$, we were able to evaluate the effective optical gap Ej_g^{eff} in the GeO(solid) films and in the GeO_2<Ge-NCs> heterolayers formed upon decomposition of the films. The variation of the effective optical gap in GeO(solid) films with the growth of annealing temperature T_{an} is shown in Fig. 9. For comparative analysis of obtained Ej_g^{eff}– values and for analysis of Ge-nanocluster sizes, the values of Ej_g^{eff} for amorphous bulk germanium and for GeO_2<Ge-NCs> heterolayers are also shown in Fig. 9, curves 5 and 6. For the effective optical *gap* $E^5{}_g^{eff}$ in GeO_2<Ge-NCs> heterolayers, a value of 1,15 eV was found, and the mean size of Ge NCs in the heterolayers proved to be ~5 -6 nm (according to TEM data). Since the value of Ej_g^{eff} in annealed GeO(solid) films always remained appreciably higher than 1,15 eV, it can be concluded that a-Ge nanoparticles in those films were smaller than nanocrystal sizes in GeO_2<Ge-NCs> heterolayers. These data have also allowed us to evaluate the sizes of a-Ge nanoparticles in other examined films.

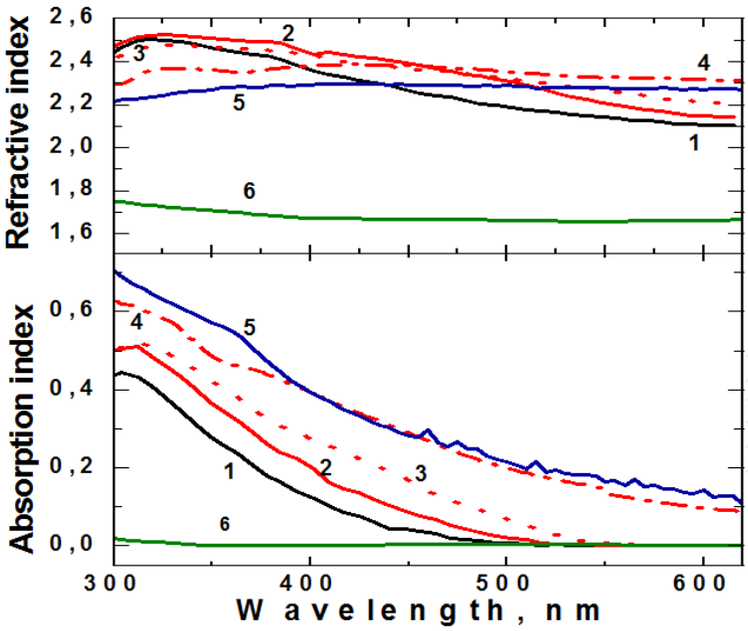

Figure 8. Spectral dependences of optical constant (n(λ) and k(λ)) in the various films: 1, 2, 3, 4 – as-deposited GeO(solid) film and films annealed at 260, 290, and 320 °C, 5 – LP CVD GeO_2<Ge-NC> heterolayer, 6 - thermal GeO_2 film grown on a single-crystal Ge(111) substrate.

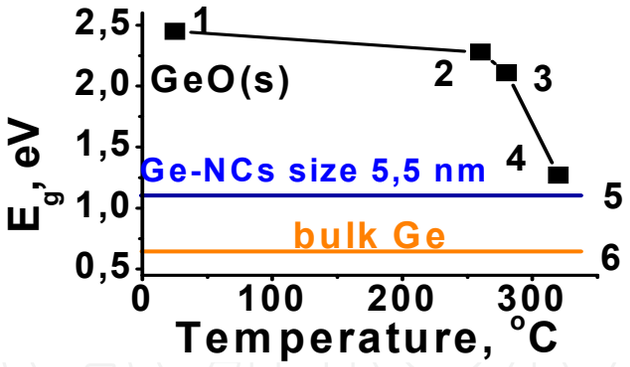

Figure 9. The effective optical bandgap E^{eff}_g versus annealing temperature: **1** – in as-deposited GeO(solid) films (with Ge-NCs sized 0,2 - 0,4 nm) and after subsequent anneals (**2** - 260 °C, 6 min; **3** - 290°C, 4 min, **4** – 320°C, 4 min); **5** – E^{eff}_g for a GeO_2<Ge-NCs> heterolayer with 5,5-nm Ge NCs; **6** - E^{eff}_g for bulk Ge.

According to AFM data, on a sample area irradiated with one laser pulse the shrinkage degree of the film was ~5 - 9%; this value increased up to ~23 - 34% under four laser pulses (Figs. 10 and 11). The cause for the film shrinkage was the low initial density of the film conditioned by the presence of many defects in the atomic network of GeO(solid). Similar data were also obtained for GeO_x layers covered by a cap SiO_2 layer (on a silicon substrate) in which the predominant part of the GeO(solid) component has already decayed during the growth of those layers. Notable film shrinkage is usually observed on anneals in loose films grown by CVD at low temperatures. Normally, thermal treatments modify the structure of CVD films and improve their quality. Anneals of multilayer structures activate both the shrinkage processes in individual layers of multilayer films and the chemical reactions proceeding among neighboring layers (Knoss, 2008). The high defect content alleviates mass transfer processes in the layers and rearrangement of their structure.

4.1.2. Changes in the structure and properties of thin bilayer coatings under ns PLA

Raman spectroscopy and microprobe IR-spectroscopy were used to analyze the structure of germanium inclusions in examined films. The non-destructive Raman method combined with calculations is a very informative tool for nano-object studies. The presence of Raman peaks at 301,5 and 520 cm^{-1} in the spectra is an indication of c-Si and c-Ge micro-inclusions present in the layers in which light is scattered by long-wave lattice phonons. It is in this way that micro- and nanoparticles are usually detected in the films of these materials. By the way, if the crystals are small-sized (~nm), then the spectral position of related Raman peaks exhibits a red shift in comparison with the spectral position of the peaks due to bulk c-Si and c-Ge. According to the peak shift value, one can determine the mean size of semiconductor nanocrystals in the films of interest using the phonon localization method (Volodin et al., 2005). The greater is the Raman shift of the peaks toward smaller wavenumbers in comparison with the position of the peaks in bulk c-Ge (301,5 cm^{-1}), the smaller is the typical size of Ge nanocrystals in the films (Fig. 12). Broad scattering bands peaking at 275 - 280 cm^{-1}, which are due to the presence of amorphous germanium, are also clearly seen in the Raman spectra of examined GeO(solid) films and GeO_2<Ge-NCs> heterolayers since it is into

this spectral region where the maximum density-of-state value of optical vibrations in a-Ge falls. In the films under study, amorphous germanium is normally contained in the form of nanoparticles dispersed in glassy GeO_2 matrix (Knoss, 2008).

The decrease of film thickness and increase of film material density after PLA as manifested in the Raman spectra of Si/GeO_2<Ge-NCs>/SiN_xO_y films is accompanied with the growth of the intensity of the peak at 520 cm^{-1} due to light scattering by long-wave optical phonons

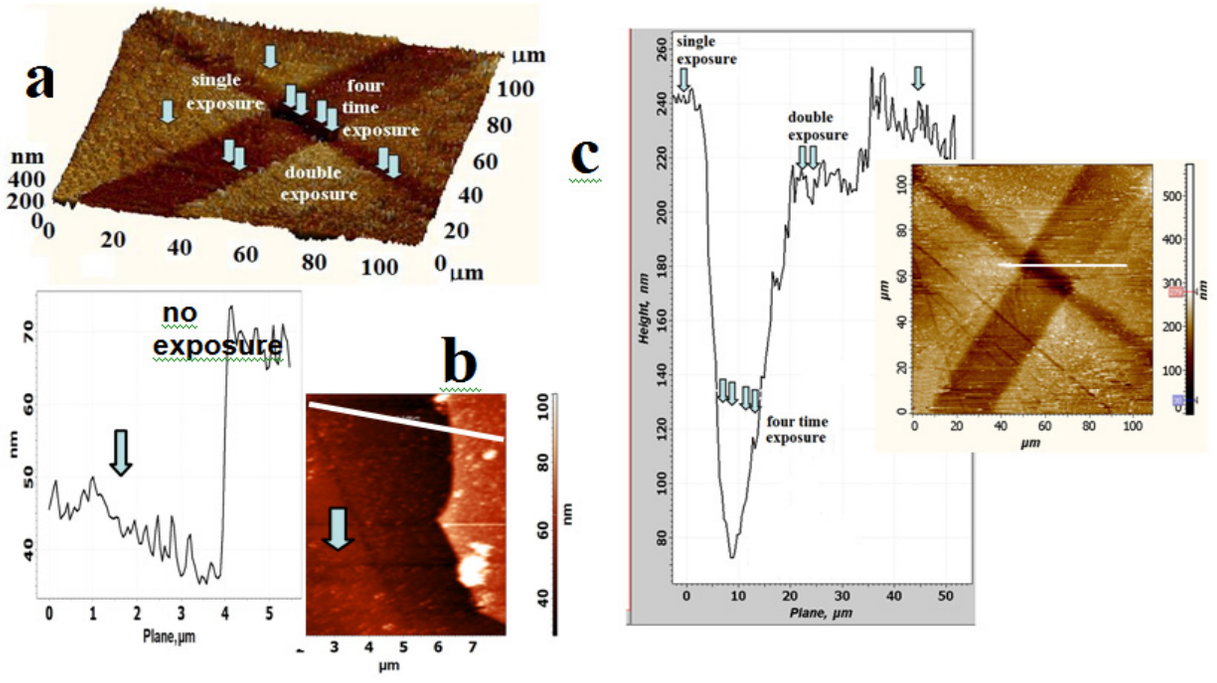

Figure 10. **a** - AFM image illustrating the shrinkage of the GeO_2<Ge-NCs>/SiN_xO_y bilayer system in region 2 (see Fig. 7 b) after PLA of the sample with ns laser pulses (fluence E_0=150 mJ/cm^2); **b -** measurements of the shrinkage of the bilayer film in the region treated with one laser pulse, **c** – the same for two and four laser pulses. The arrows ↓, ↓↓ and ↓↓↓↓ indicate regions subjected to the single, double and four-time exposures.

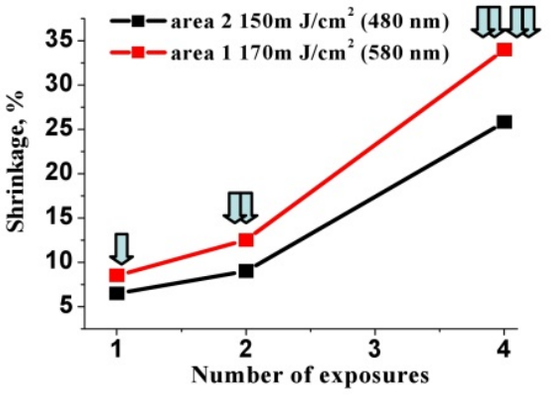

Figure 11. Effect of the number of laser pulses, laser fluence, and thickness of GeO_2<Ge-NCs> heterolayer on the shrinkage value of the Si/GeO_2<Ge-NCs>/SiN_xO_y bilayer system.

in the Si substrate (Fig. 12). This effect is manifested as an increase of the transparency of the bilayer film for the excitation laser radiation in Raman measurements (514,5 nm Ar+ laser) falling onto, and reflected by, the substrate. The cause for the shrinkage effect are PLA-induced changes of optical constants of the films in the Si/GeO_2<Ge-NCs>/SiN_xO_y bilayer system, as optical constants of Si substrate remained essentially unaltered in the spectral region around the excitation wavelength. Let us consider now possible reasons for such changes. Some minor increase in the refractive index of a very thin SiN_xO_y film due to its shrinkage and compaction cannot be the factor appreciably affecting the optical constants of the bilayer system. The absorption index of the film in this spectral region is initially very small, and the irradiation of the sample with laser radiation could not considerably increase its value. Hence, the increase in transparency of the bilayer system was most probably due to the change in the optical constants of the GeO_2<Ge-NCs> heterolayer or, alternatively, it could be a result of the chemical interaction of the two layers in the interfacial region of the structure.

Indeed, micro-Raman and micro-IR-spectroscopy data showed that such processes indeed proceed in the film system under study. Raman spectra taken from local areas of the film system irradiated with one, two, or four laser pulses (see Fig. 12 a) were measured with excitation laser beam focused to a ~1-μm diameter spot on the sample surface. From the registered changes in Raman spectra, we were able to judge the rate of release of Ge atoms during decomposition of the GeO(solid) structure, and also the formation of amorphous (α-Ge) and, then, crystalline (c-Ge) phases of Ge. The formation kinetics of α-Ge and c-Ge phases within the heterolayer is characterized by initially the highest amorphous germanium content of the layer system and by almost complete absence of c-Ge phase from it (see the initial spectrum in Fig. 12 a). After one laser pulse, the fraction due to α-Ge component sharply decreased in the system, and c-Ge phase emerged in quite large quantities. Two and four laser pulses gave rise to an increased amount of c-Ge phase at a comparatively slow regeneration of α-Ge component. During annealing in these

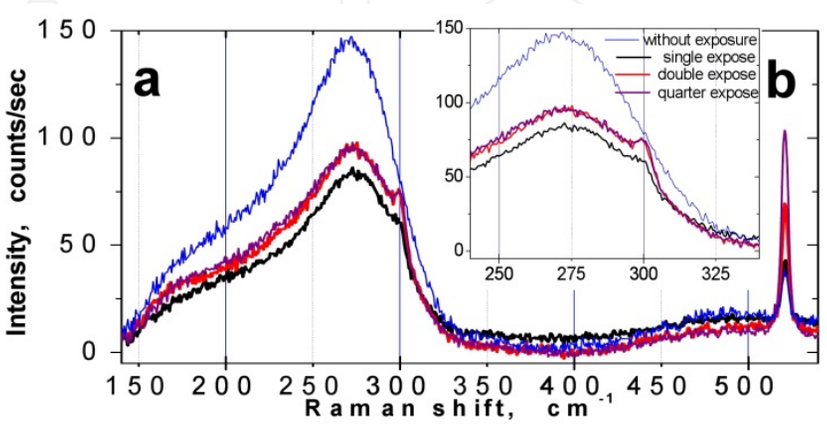

Figure 12. **a** - Raman spectra illustrating the influence of the number of ns laser pulses given to a local region on the sample (region 2 in Fig.7 b, E_0 =150 mJ/cm²) on the structure of the GeO_2<Ge-NCs> heterolayer in the Si/GeO_2<Ge-NCs>/SiN_xO_y bilayer system; **b** – magnified fragment of the same spectra.

heterolayers, amorphous germanium phase usually forms a big amount of amorphous Ge nanoparticles growing in size during high-energy treatments of the system, and then such nanoparticles undergo crystallisation without interrupting their continuous growth. The growth of Ge nanoparticles proceeds primarily due to decay of nanocluster fractions with minimal sizes. The formation processes of α-Ge and c-Ge nanoparticles are also maintained by the decay of the atomic network of metastable GeO(solid), which supplies the nanoparticles with atomic germanium.

According to micro-IR-spectroscopy data (Fig. 13), the atomic network of the insulator matrix also undergoes modifications that proceed simultaneously with the transformation processes of germanium inclusions in the GeO_2<Ge-NCs> heterostructure. Yet, the process turned out different than the expected formation of pure glassy GeO_2 by reaction (3) during anneals of GeO(solid) films (Fig. 4 b). In the heterolayer region treated with one laser pulse the IR absorption band starts moving towards longer wavelengths instead of showing the expected trend to the maximum at 860-870 cm^{-1}. On the other hand, the maximum IR absorption intensity in the region treated with two laser pulses decreases markedly, and the whole band notably widens. In the bilayer structure under study, in addition to the formation of GeO_2 during decomposition of metastable GeO(solid), the GeO_2<Ge-NCs> heterolayer and the SiN_xO_y film can react with each other in the interfacial region. The GeO_2 matrix of the heterolayer, and the Si_3N_4 and SiO_2 materials forming the cap SiN_xO_y layer, are involved in this reaction. In particular, the products of the reaction between GeO_2 and Si_3N_4 proceeding at T>650^{0}C ($3GeO_2 + Si_3N_4 \rightarrow 3SiO_2+Ge_3N_4$), SiO_2 and Ge_3N_4, can be dissolved by glassy GeO_2 matrix. As described above, these processes finally yield a GeO_2:SiO_2:Ge_3N_4→ k:p:q glassy compound. Since pure Ge_3N_4 and glassy SiO_2 exhibit IR absorption peaks respectively at about 770 cm^{-1} and 1070 cm^{-1}, it can be expected that the peaks due to the Ge_3N_4:GeO_2 and GeO_2:SiO_2 double glasses will tend to shift in opposite directions from the peak due to pure GeO_2; i.e. the first peak will shift towards longer wavelengths and the second peak, towards shorter wavelengths. On the whole, the material of the GeO_2 matrix is expended on the formation of both SiO_2 and Ge_3N_4, and also on the formation of the three-component GeO_2:SiO_2:Ge_3N_4 → k:p:q compound. As a result, a predominant part of the cap SiN_xO_y layer may turn into Ge_3N_4 and SiO_2 that will subsequently undergo dissolution in the upper part of the GeO_2<Ge-NCs> heterolayer. Such transformation will be capable of reaching depths comparable with the thickness of the initial cap layer. This may become the reason for the observed modification of the IR absorption band in the irradiated film, including reduced absorption at the band maximum, shift of the band, and its strong widening (Fig. 13).

Of course, the properties of the upper layer in the initial bilayer structure will undergo dramatic changes. In particular, the optical constants and the optical bandgap will strongly change in this layer. Dissolution of wide-bandgap glassy SiO_2 (E_g^{SIO2} ~ 9 eV) in the matrix of the GeO_2<Ge-NCs> heterolayer will radically change the energy-band characteristics of the heterosystem. A similar behavior is also demonstrated by glass-like Ge_3N_4, which is close to GeO_2 in terms of optical gap, E_g^{Ge3N4} ~ 5-5,5 eV, yet differs from GeO_2 in its high refractive index (1,90-2,00) and permittivity (~9-11). On the contrary, the refractive index of SiO_2 (1,45) is lower than that of glassy GeO_2 (1,61-1,63) (Gorokhov, 2005).

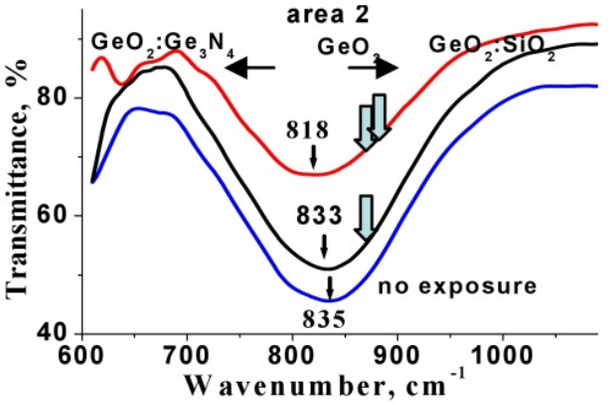

Figure 13. Micro IR transmittance spectra illustrating the influence of the number of ns laser pulses given to a local region on the sample (region 2 in Fig.7b, E_0 =150 mJ/cm^2) on the structure of the dielectric in the Si/GeO_2<Ge-NCs>/SiN_xO_y bilayer system.

The degree of compositional changes in the upper part of the layer will depend on material viscosity. In the described process, this degree will grow from one to the other irradiation pulse as regions with altered chemical composition will spread away from the interface across both films of the bilayer system. In turn, the compaction of the material in each layer will more and more impede the diffusion process in the intermixing region of the bifilm. Formation of fine cracks at the periphery of the squares irradiated with laser pulses serves an indication for the growth of viscosity in the upper part of the bilayer structure. The formation process of such cracks is defined by two factors: (i) growth of the internal tensile stress in the film due to material compaction (the shrinkage of the film in the direction normal to the film plane does not completely eliminate the lateral internal tensile stress in the film) and (ii) growth of viscosity in the compacted layer due to increase of strength characteristics of the material proceeding with simultaneous vanishing of defects from the atomic network and with modification of the chemical composition of the layer (Gorokhov et al., 1998). As a result, quite a thick intermediate layer (up to ~50-80 nm), in which the insulator matrix has a variable chemical composition and altered structural, mechanical, physical and other material properties, forms during the reactions at the interface between the GeO_2<Ge-NCs> heterolayer and the SiN_xO_y film. There are no Ge nanoparticles in the upper part of this layer, but the concentration of such nanoparticles gradually increases as we approach the pure GeO_2<Ge-NCs> heterolayer. The optical constants of the upper layer, as well as its optical gap value, also vary in a complex manner over the thickness of the layer. But, since glassy SiO_2, a very broad-band material, presents one of the composite-glass components, the optical gap in the mixture will be everywhere wider than the optical gap in the regions where only narrow-band glassy components, having an optical gap not wider than 5 - 5,5 eV, are present. Hence, in the course of PLA treatments of the samples with KrF excimer laser pulses the upper multi-component layer will become increasingly more transparent to the excitation beam of the Ar+ laser (514,5 nm) in comparison with the bulk of the lower GeO_2<Ge-NCs> heterolayer.

Note that all the discussed processes can be realized using traditional heat treatments at T≥ 400^0C. Yet, the duration of such heat treatments is typically greater than one minute, whereas, in our case, many atoms simultaneously participated in several structural-chemical rearrangement processes for only several tens of ns. To gain an insight into the whole picture of involved processes, let us focus on their most important features. First, AFM data on the shrinkage of the layered structure and IR-spectroscopy data on the modifications of its chemical composition reveal a gradual increase in the rate of structural-chemical transformations in the system from the first to last laser pulse (Fig. 11). Second, the dynamics of irradiation-induced changes in the optical properties of the bilayer film shows a distinct saturation. Those changes first occur rapidly and, then, their rate sharply decreases. The latter is evident from changes in the Raman spectra of the Si/GeO_2<Ge-NCs>/SiN_xO_y system observed 275 to 300 cm^{-1} (Fig. 12 a) at the beginning and at the end ot its irradiation with a sequence of ns laser pulses. During the first pulse, the input energy was absorbed more readily by the bilayer film in comparison with subsequent pulses since the changes in the Raman spectra due to the first pulse were manifested more distinctly in comparison with the changes induced by the second pulse and, the more so, by the two subsequent pulse. The successive growth of the intensity of the Raman peak (520 cm^{-1}) due light scattering by the lattice of Si substrate for Ar+ laser excitation (Fig. 12) also agrees with the general tendency in pulse-by-pulse modification of film-structure properties although, here, a more steady growth of peak intensity is observed. The effect is explained by an increase of bilayer film transparency, or reduced absorption of laser radiation by the film in this spectral region). A common feature for all pulses was that a predominant part of their energy dissipating in GeO_2<Ge-NCs> was spent on rearrangement of its lattice structure that proceeded mainly during the time intervals between the pulses.

An unusual thing here is that, with each subsequent radiation pulse, the Si/GeO_2<Ge-NCs>/SiN_xO_y hetrosystem becomes more and more transparent to the probing Raman-spectrometer radiation. Initially, we expected quite a contrary thing, namely, an increase in the absorption of Ar^+ laser beam radiation by the GeO_2<Ge-NCs> heterolayer. Such an increase was expected to be a result of the considerable amount of free Ge atoms released in the heterolayer bulk. Ge atoms become the material for nucleation and growth of many Ge-nanoparticles, which was to be manifested as an increased absorption coefficient of the heterolayer in the visible spectral region. For instance, such a growth of the absorption coefficient was observed during successive anneals of GeO_2<Ge-NCs> heterolayers and GeO(solid) and GeO_x films (Fig. 8). Similarly, during growth of silicon nanoparticles in the bulk of non-stochiometric SiO_x and Si_xN_y(H) films under chemical and laser treatments no enhanced transparency of such films was observed in the visible spectral region (Korchagina et al., 2012; Rinnert et al., 2001; Volodin et al., 2010). However, it proved to be a very difficult task to reveal the true nature of such an unusual effect in the experiments with the bilayer system under study, as in PLA-treated samples several different chemical and structural processes proceed simultaneously in the bulk of the GeO_2<Ge-NCs> heterolayer and at its boundaries. It was required to simplify the complex of such structural and compositional modifications in the films. Therefore, we first undertook an analysis of material

transformations proceeding during traditional heat treatments in a GeO(solid) film on Si substrate without cap layer (ISP SB RAS) and in a GeO_x film on Si substrate protected by a cap layer formed from sputtered SiO_2 (~100 nm) (Nancy University, France).

A GeO(solid) layer of uniform thickness 61 nm was characterized with the follows values of optical constants: n=1,86 and k=0 (obtained from many-angle ellipsometric measurements using an He-Ne laser with λ=632,8 nm at beam incidence angles 45^0, 50^0, 55^0, 60^0, 65^0, and 70^0). A broad band peaking at 280 cm^{-1} due to Ge nanoparticles was observed in the Raman spectra of the as-deposited film (Fig. 14). The film was thin and its decomposition just began; therefore the amplitude of this Raman band was very low, especially at the sample edges (spectrum 3) where the film was less heated by the evaporator during the film deposition process. The highest degree of decomposition of the GeO(solid) film was observed at the centre of the sample (spectrum 2). Note that 4-minute exposition of a local sample area to the excitation laser beam focused to a ~1-μm diameter spot on the film surface at the centre of the sample caused a strong reduction in the beam scattering by a-Ge nanoparticles (spectrum 4). This effect was due to photo-stimulated oxidation of the particles by air oxygen in the locally heated surface area. Here, the concentration of a-Ge nanoparticles decreased in the film; yet, the film thickness grew in value due to the formation of an additional amount of germanium dioxide in the film. A comparison of the Raman spectrum of Si substrate without a film (spectrum 1) with the other spectra in Fig. 14 shows that deposition of a GeO(solid) layer onto the film surface (spectrum 3), growth of the fraction of a-Ge in the film in the form of nanoparticles (spectrum 2), and transformation of part of a-Ge nanoparticles into glassy GeO_2, i.e. increase in the volume of heterolayer matrix (spectrum 4) lead to multiply decreased amplitude of the peak at 520 cm^{-1} in the Raman spectrum of the Si/GeO(solid) system, this peak being due to light scattering by long-wave optical phonons in the Si substrate. The latter finding can be attributed to enhanced absorption of Ar^+ laser radiation in the GeO(solid) film for all these cases.

The cap layer prevents evaporation of the GeO_x layer in $Si/GeO_x/SiO_2$ structures (with layer thicknesses 100 nm/100 nm) annealed at temperatures $T>450^0C$. As a result, the initial metastable atomic network of GeO(solid) in such structures undergoes decomposition with the emission of all the excessive germanium and its accumulation in a-Ga nanoparticles. On increasing the annealing temperature, such a-Ga nanoparticles transform in Ge nanocrystals. These processes can be easily monitored using Raman scattering measurements (see Fig. 15). The temperatures used to anneal the $Si/GeO_x/SiO_2$ sample were insufficient for the onset of a reaction between the GeO_2 matrix in the decomposed GeO_x film and the SiO_2 cap layer; this sample was found to also not absorb the Ar+ laser radiation and undergo no heating due to the wide optical gap of the material. Hence, all the changes proceeding with the Raman scattering peak due to light scattering by phonons in Si substrate bear no relation with modification processes in the structure of the GeO_x layer. On the other hand, it is seen that the process of germanium release in the GeO_x film proceeding with the formation of a-Ge nanoparticles and their subsequent crystallisation successively reduces the amplitude of the peak due to Raman scattering in Si substrate. The same result was also observed in deposition of the initial GeO_x layer, like in the case of GeO(solid) layer synthesis (see Fig.14).

Note that the spectral position of the Raman peak due to Ge-nanocrystals in the GeO_x film is no difference from the spectral position of the peak in bulk Ge crystals (301 cm^{-1}). The latter finding is indicative of rather large mean sizes of Ge nanocrystals (~8-10 nm and greater) formed in this film during anneals.

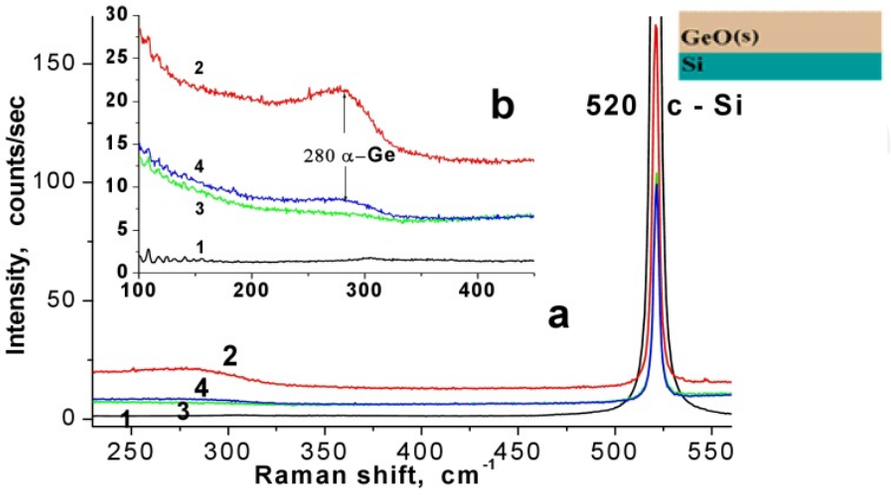

Figure 14. **a** –Raman spectra of GeO(solid) films of different thicknesses after decomposition of GeO(solid) into GeO_2 and Ge nanoclusters and oxidation of the nanoclusters: **1** – Si substrate, **2** and **3** - thick and thin areas of the GeO(solid) film, **4** - thick area of the GeO(solid) film where Ge nanoclusters were oxidized by the Ar + laser; **b** – magnified fragments of the same spectra.

Thus, the experiments with GeO(solid) and GeO_x films showed that the modification processes of their structures proceeding during traditional anneals are qualitatively similar to PLA-induced processes. All such processes (film shrinkage and densification, all decomposition stages of the metastable GeO(solid) atomic network, formation of a-Ge nanoparticles and their oxidation and crystallisation) do not make the layers more transparent for Ar^+ laser excitation radiation. Among all the above-considered physicochemical processes in the analyzed one- and bilayer compositions, only reactions of the glassy GeO_2 matrix in GeO_2<Ge-NCs> heterolayers with Si_3N_4 cap layers could lead to such an effect. Besides, the decrease of the Raman-spectrometer beam absorption in the Si/GeO_2<Ge-NCs>/SiN_xO_y system with increasing the number of ns KrF excimer laser pulses given to the sample (Fig. 12) could be explained assuming that a-Ge nanoclusters formed by short laser pulses in the GeO_2<Ge-NCs> heterolayer were substantially smaller than a-Ge nanoclusters formed during traditional thermal treatments. Thus, the whole mass of free Ge atoms leaving the decaying atomic lattice of GeO(solid) during irradiations formed a multitude of very small c-Ge nanoparticles.

The latter is quite natural a situation under conditions of abrupt heating of the heterolayer not only with laser impulses, but also with the energy released during decay of the unstable atomic network of GeO(solid) undergoing decomposition during the discussed treeatments. However, due to the short width of laser pulses, the length of possible diffusion of free Ge toward Ge nanoclusters does not exceed 2-3 cluster diameters, as nanoclusters are separated with distances close to the mean radius of nanoclusters in studied heterolayers. Hence, in

small-sized a-Ge nanoparticles, due to the 3D quantum confinement effect, the effective optical gap will be substantially wider than that of larger nanocrystals formed during traditional anneals and, hence, their radiation absorption effect will not be so high as that of the larger Ge nanoparticles.

The sensitivity of our Raman spectrometer has allowed us to reveal in our experiments specific features directly defined by the sizes of Si and Ge nanocrystals in thin-film materials (Volodin et al., 2005). In large Ge nanocrystals, the spectral position of the Raman peak is at 301,5 cm^{-1}, with its blue shift becoming notable at nanocrystal sizes < 6-7 nm. Data on the spectral position of the Raman peaks due to Ge nanocrystals hosted in a GeO_2 matrix as calculated from two theoretical models (data of (Nelin & Nilsson, 1972) and data calculated from the model of effective density of folded vibration states (Volodin et al., 2005)) are shown in Fig. 16. Raman spectra of irradiated GeO_2<Ge-NCs> heterostructures measured in the spectral region around the wavenumber 301,5 cm^{-1} are shown in Fig. 12 b. In these spectra, a red shift of Raman peaks, typical of Ge NCs, is clearly observed. According to model calculations, the sizes of Ge NCs increase from 1,4 – 1,8 nm to 1,8 – 2,3 nm (Fig. 16)

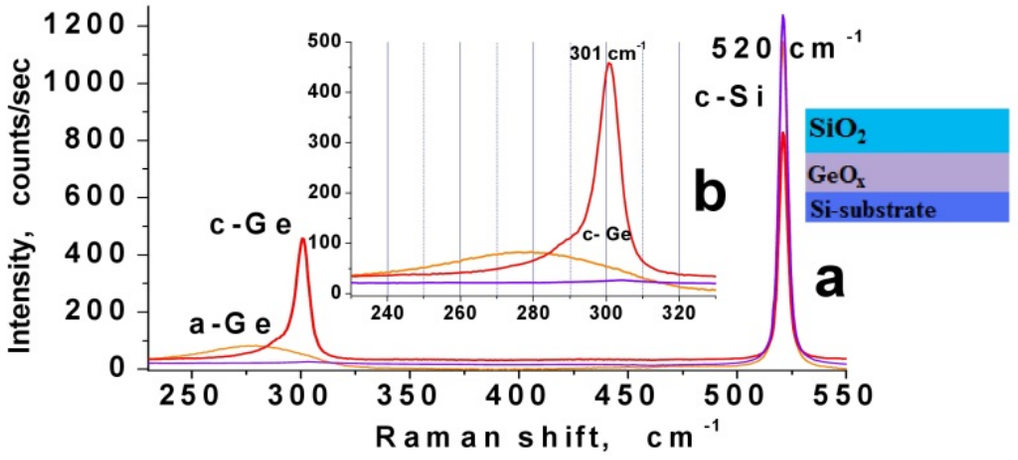

Figure 15. **a** - Raman spectra of a SiO_2/GeO_x/Si (100/100 nm) structure illustrating the precipitation of germanium in GeO_x layers during anneals, and also the formation of a-Ge nanoparticles and their subsequent crystallisation: **1** - as deposited film; **2** and **3** – films annealed at 300 °C for 40 min and at 480 °C, 3 min + 530 °C, 1 min, respectively; **b** – the same spectra at a larger magnification.

with increasing the number of ns KrF excimer laser pulses given to local regions on the sample surface. This result confirms the previous assumption on the reason for transparency enhancement for Ar+ laser radiation in GeO_2<Ge-NCs> heterolayers irradiated with 25-ns KrF excimer laser pulses (λ=248 nm).

Note that analogous treatments of non-stochiometric silicon-rich SiO_x and Si_xN_y(H) glassy films with high-energy KrF excimer laser pulses (λ=248 nm, t_p=25 ns) activate a complex structure rearrangement process which begins with the emission of excessive Si atoms from the atomic network of the material due to breakage of Si-O bonds (in SiOx films) or Si-H and Si-N bonds (in Si_xN_y(H) films). The process ends with the formation of many a-Si nanoparticles in the film bulk from released Si atoms followed with subsequent

crystallization of the nanoparticles (Gallas et al., 2002). In such cases, the silica films undergo shrinkage. Here, all processes proceed like in GeO_2<Ge-NCs> heterolayers. However, unlike in the latter case, in PLA-treated GeO_2<Ge-NCs> heterolayers there is no growth of transparency for Ar^+ laser radiation; on the contrary, according to (Korchagina et al., 2012), the absorption of 514,5-nm radiation increases. Today, the reason for the different behaviors demonstrated by the GeO_2<Ge-NCs> and SiO_2<Si-NCs> systems under PLA treatments remains unclear. In this effect, which depends on many factors, the contribution due to each factor changes under PLA differently in Ge- and Si-based heterosystems.

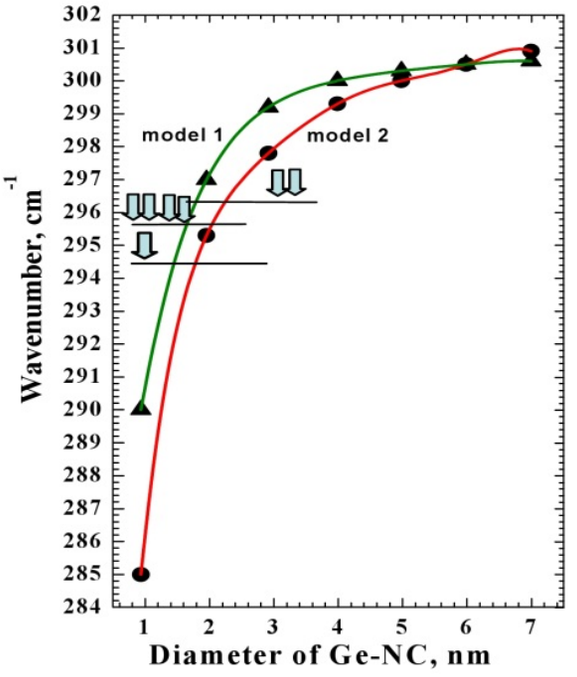

Figure 16. The spectral position of the Raman peak due to Ge nanocrystals versus nanocrystal size in GeO_2<Ge-NCs> heterolayers: ● – data of (Nelin & Nilsson, 1972), ▲ - data calculated by the model of effective density of folded vibration states (Volodin et al., 2005). Using the Raman spectra in Fig. 12, one can determine the sizes of Ge NCs size formed in local areas of the GeO_2<Ge-NCs>/ SiN_xO_y bilayer system treated with one, two and four ns laser pulses.

Finally, we would like to emphasize here that irradiation of samples with 25-ns KrF excimer laser pulses (λ=248 nm) produces a very important effect on GeO_2<Ge-NCs> heterolayers, namely, its allows one to decrease both the sizes and size dispersion of Ge nanoparticles formed in metastable GeO(solid) and GeO_x layers. This process proceeds in the strongly densifying GeO_2<Ge-NCs> heterolayer that consists of 70% vol. of GeO_2 matrix, which, during the same irradiation treatment, is capable of controllably changing its chemical composition, structure, and physical, optical and electrophysical properties.

4.2. Femtosecond treatments of samples with Ti-Sapphire laser

Differences in laser radiation parameters, and also differences in other irradiation conditions, strongly affect the material modification process and its ultimate results. The

idea of to which extent the final effect due to PLA might differ in various irradiated systems can be grasped through making a comparison of PLA data for film structures involving GeO, GeO_x layers, and GeO_2<Ge-NCs> heterolayers obtained in treatments performed using two different lasers, a KrF excimer laser and a Ti-Sapphire laser.

Phase transition mechanisms in solid materials under femtosecond laser treatments are radically different from analogous PLAs implemented using nanosecond pulses. These differences are most clearly manifested in the case of ultra-high-power femtosecond laser treatments, when nonlinear effects play an important role in the light absorption processes. There are many contributions devoted to the study of the interaction of femtosecond laser pulses with matter (Juodkazis et al., 2009). Results of an experimental study of the dynamics of electron-hole plasma formation and recombination of photo-induced charge carriers in Si under fs PLA at laser energy lower the threshold value for surface melting and ablation were reported by Ashitkov et al. (Ashitkov et al., 2004). During the action of a fs laser pulse, electron-hole plasma with electron concentration in the conduction band up to 10^{22} cm^{-3} forms, both thermally activated and athermal surface-layer melting processes being observed along with a transition of material to metallic state. In (Ashitkov et al., 2004), time-dependent optical reflection was measured for heating-pulse energies.

In phase transitions under such conditions, athermal effects may emerge. Indeed, the duration of fs laser pulses is much shorter then the duration of the electron- phonon interaction in semiconductor (approx. 1-2 ps). That is why in silicon, during laser pulse the "hot" electron-hole plasma does not excite vibrational modes and relaxes insignificantly. The temperatures of the electron and atomic sub-systems are much different. According to theoretical calculations, the material becomes unstable when the electron concentration excited from the valence to conduction band reaches 9-20% of the atom concentration in Si lattice (Bok, 1981). This metastable state may relax to a more stable crystalline phase without melting yet with release of latent crystallisation heat. The process is similar to "explosive" crystallisation. In several picoseconds after the pulse, the phonon and electron temperatures should equalize. Post-pulse processes, e.g. post-pulse atomic diffusion in heated films, start manifesting. Very probably, diffusion can be stimulated by laser radiation not only via film heating, but also due to the breaking of valence bonds that occurs when electrons undergo excitation to the conduction band. Under nanosecond laser treatments, the time of Si film cooling to a temperature below the melting point is known to amount to about 100 nanoseconds (Sameshima & Usui, 1991). For fs laser treatments, the cooling time can be expected to be the same. This time can turn out sufficient for diffusion of excess silicon and for formation of nanocrystals only in the case of melt.

Zabotnov et al. (Zabotnov et al., 2006) showed that femtosecond laser annealing of Si surfaces leads to their nanostructuring, two types of formed nanostructures being observed. In one case, these are ordered lattices with a period somewhat shorter than laser radiation wavelength. The formation of such structures can be explained by the interference between the fs radiation waves and the non-equilibrium plasma excited by radiation in the surface layer. Here, ablation of Si atoms is accompanied with their rapid oxidation in air, and also with the formation of surface Si nanocrystals sized 3-5 nm.

Martsinovsky et al. (Martsinovsky et al., 2009) showed that, under the action of femtosecond laser pulses, intense photo-excitation of semiconductor surface, which dramatically modifies its optical response and provides conditions for generation of surface electromagnetic waves of various types, becomes possible. Martsinovsky et al. have also discussed the interrelation of electronic processes optically induced in the near-surface layer with the formation of periodical surface microstructures that were observed in experiments on irradiation of silicon targets.

Femtosecond PLAs were also used to crystallise silicon films. In PLA treatments, a critical point for thin films is proper choice of irradiation conditions since at high pulse energies such films may readily suffer ablation. At present, the issue of Si-nanocrystal formation in silicon nitride and silicon oxide films under nanosecond PLAs is a well-studied matter. A process for fabricating nanocrystals in dielectric films with the the help of nanosecond laser pulses was patented as involved in the production technology of non-volatile flash memory devices. Femtosecond treatments were used for modification of Si nanoclusters in SiO_2 films (Korchagina et al., 2012). Yet, for femtosecond treatments structural changes in silicon clusters in SiN_x and SiO_x films have not been studied. As for germanium, Ge films, and Ge nanoparticles embedded in dielectric layers, to the best of our knowledge, only one reported communication on fs-laser-initiated crystallisation in thin layers of amorphous Ge is presently available (Salihoglu et al., 2011).

On the whole, the physics underlying processes in film systems subjected to to femtosecond anneals still remains scantily understood. That is why it would be interesting to perform a study of such processes in samples treated with nanosecond and femtosecond laser pulses with revealing all involved characteristic features, also including possible athermal effect on Ge nanoparticles hosted in an insulator matrix, both with the aim of detecting new manifestations of PLA-induced effects in germanium-based materials and with the aim of comparison of similar processes in systems based on two chemically akin semiconductors, Si and Ge. Assumes that the results of these studies will prove also useful for applications.

4.2.1. Femtosecond PLA of GeO_2<Ge-NCs> heterolayers

Our study of fs PLA-treated thin-film systems based on germanium oxide layers was the first one devoted to the subject matter of interest. Therefore, the first task in such investigations was to develop a general concept of the complex effects and phenomena occurring in the film systems of interest subjected to PLAs under different conditions. In particular, we examined GeO_2<Ge-NCs> heterofilms of different thicknesses grown by the LP CVD method on (bare and CVD SiO_2-covered) silicon or quartz glass substrates. The films either had one layer and no cap layer or they were protected by a thin cap layer of PE CVD SiN_xO_y or CVD SiO_2. In another set of samples, ~ 20 – 30 nm and ~200-250 nm thick, GeO_2<Ge-NCs> layers were part of multilayer compositions where they were separated with thin (~7-10 nm) and thick (~100 nm) CVD SiO_2 layers as shown in Fig. 17 a. Scanning was made with a focused fs-laser beam at a velocity of 100 μm/s. The frequency of laser pulses was 10 pulses per 1 μm. The laser fluence (E_{pulse}) varied from 15 to 1 mJ in ~70-μm diameter

spot and from 0.028 to 0.0018 mJ in 1-μm diameter spot. In the experiments, samples with GeO_2<Ge-NCs> heterolayers were used. In addition, in some cases optical bench vibrations of ~1,5-μm amplitude in two dimensions, in the plane of the optical bench and in the direction normal to it, were implemented. A typical result for layered systems with GeO_2<Ge-NCs> heterolayers on Si substrate scanned with Ti-Sapphire laser beam focused to a 70-μm diameter spot is shown in Fig. 17 b. From line to line, the laser fluence was decreased in 1-mJ steps within 15-mJ wide intervals of E_{pulse}. Thus, the adopted femtosecond PLA regimes and conditions for examined films were different from their treatments with the nanosecond laser in terms of the majority of basic physical parameters (laser radiation wavelength, pulse duration, intervals between pulses, arrangement of the irradiation process). Besides, in the case of fs PLAs the adopted irradiation technique did not allow us to trace changes in the film structure following successive irradiations of the sample with a series of laser pulses.

The first result was that optical microscopy was quite a sensitive technique allowing us to reveal both changes in the surface relief and the variations in the optical parameters of the material induced by structural and chemical modification processes proceeding in heterolayers under laser beam treatments, whereas the SEM method was efficient only when studying surface morphology modifications (cp. Figs. 17 a and b). The main fundamental difference in the PLA mechanisms for the two lasers is manifested when the

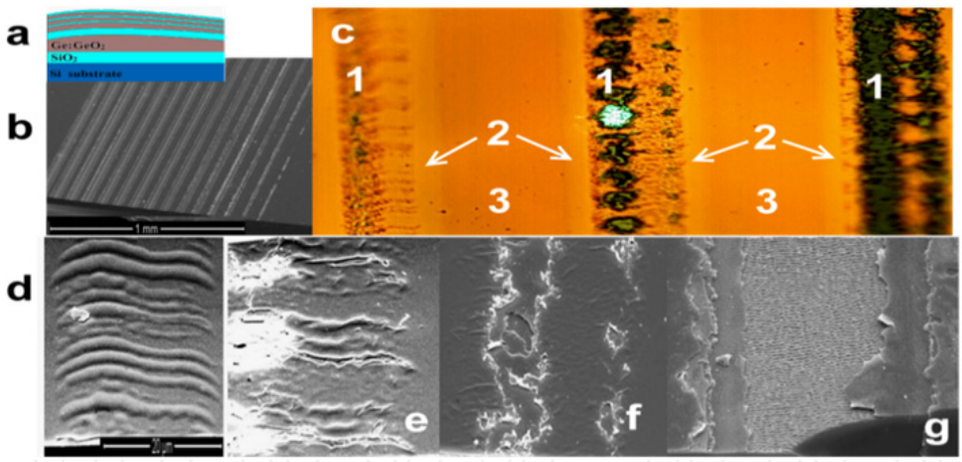

Figure 17. Surfaces of multilayer coatings involving alternating GeO_2<Ge-NCs> heterolayers and SiO_2 layers after fs PLA (beam diameter 70 μm): **a** – schematic of the multilayer coating (similar to that in Fig. 6); **b** – SEM image of the film coating treated with laser pulses of various energies; **c** – optical microscopy image of the same sample: (1) evolution of surface morphology at the centerline of laser spot path; (2) along coating edges there is no relief, although light stripes defined by the changes of optical properties of some layers inside the coating are clearly seen; (3) laser treated paths are separated with wide stripes where the film coating structure has remained unchanged (E_{pulse} was not high enough); **d**, **e, f** and **g** – SEM images obtained at the various stages of the coating laser damage process implemented with laser energy increase: **d** – development of a wavy surface relief as a result of transformation of 3 thin GeO_2<Ge-NCs> heterolayers in the top tier into nanofoam (E_{pulse} = 8 μJ); **e** - beginning of layer destruction in the top tier (E_{pulse} = 9 μJ); **f** – simultaneous damage of upper and middle tiers (E_{pulse} = 10 μJ); **g** – simultaneous damage of all layers down to the Si substrate and the beginning of its damage by formed ripples (E_{pulse} =13 μJ).

laser are used to modify GeO_2<Ge-NCs> heterolayers. Only Ge-nanoclusters, whose optical gap E_g^{eff}(Ge-NC) < 2 eV, absorbed femtosecond laser radiation with λ=800 μs in GeO_2<Ge-NCs> heterolayers (see Figs. 8 and 9). Nanosecond KrF laser radiation with λ=248 nm is additionally absorbed by the GeO_2 matrix, which constitutes 70% of the heterolayer volume, its optical gap being E_g^{eff}(GeO_2) ~4,5-5 eV. The actions of the light emitted by the two lasers on the two material components in the heterolayers are radically different: while KrF laser radiation heats both the Ge-nanoclusters and the dielectric matrix, Ti-Sapphire lase radiation heats only Ge-nanoparticles while leaving the matrix cold. It is this difference that makes the effects due to PLA processes in GeO_2<Ge-NCs> heterolayers under irradiation with the two lasers cardinally opposite. Namely, in GeO_2<Ge-NCs> heterolayers treated with the fs laser the heated Ge-nanoclusters begin to react with the surrounding glassy GeO_2 and, during this process, the initial heterostructure transforms into a totally different kind of solid with fundamentally different physical properties.

4.2.2. Formation of GeO_2 nanofoam using fs PLA of GeO_2<Ge-NCs> heterolayers

Indeed, Ge-nanoclusters surrounded by GeO_2 matrix were rapidly heated by fs laser radiation, to which the oxide was transparent, unless the chemical reaction (4) between both components in GeO_2<Ge-NCs> heterostructure was initiated. The emitted germanium monooxide molecules (GeO(gas)) are initially localised in the vicinity of hot Ge-nanoparticles surrounded by a cooler insulator (Fig. 18). Affected by the vapor temperature and pressure, the glassy GeO_2 matrix gets heated and it extends when softening. On cooling, the GeO_2<Ge-NCs> heterostructure turns into a swelled mass of nano-dimensional glass cells. Each of the initial Ge-nanoclusters, as its grows smaller and lighter, is to remain inside a formed nano-cells (Fig. 18 c). The most surprising thing here is that, in the outcome of nano-foam formation process, all Ge-nanoparticles should have a uniform minimal size independently of their size in the initial heterolayer. Due to the 3D quantum-dimensional effect, Ge-nanoclusters, as they grew smaller during their reaction with the GeO_2 matrix, should stop absorbing the heating light according to the condition $h\nu = E_g^{eff}$(NCs). This technique allows us to obtain ensembles of isolated indirect gap semiconductors of very small dimensions that also have a low size dispersion.

The process is completed as follows. While the nano-cell sizes in the glass softened under the internal gas pressure of the gas inside grow in value, their glass walls start cooling. The latter is due to the fact that, first, the gas in the nano-cells volumetrically expands under near-adiabatic conditions and, hence, the gas temperature will decrease. In addition, the mechanical expansion of the nano-cells in the soft GeO_2 nanofoam consumes the energy from the gas in cells. The gas gives off heat and its pressure decreases. Simultaneously, the nanocell-hosted Ge-nanoclusters, as they grow smaller, start absorbing less fs laser radiation (due to the 3D quantum-confinement effect). This reduces the efficiency of the reaction yielding new portions of GeO(gas) in the nano-cells. Thus, in the nanofoam the nano-cell walls start cooling at a sufficiently high internal pressure due to GeO(gas) vapor. Cooling of the GeO_2 glass rapidly increases its viscosity, which prevents the nano-cells from being compressed with decrease of the internal GeO(gas)

pressure. Thus, the individual nano-cells, as well as all of the nanofoam, will preserve their dimensions in the cooling process.

PLA results of multilayer film systems consisting of a conventional dielectric layers and GeO_2<Ge-NCs> heterolayers illustrate in Fig.17 the complex effect of fs laser radiation on the system. The system consisted of nine layers belonging to two types: thick and thin SiO_2 films and GeO_2<Ge-NCs> heterolayers that alternated among each other (according to the diagram in Fig. 17 a). With increase of laser pulse energy, distinct indications of film structure modification started showing up, becoming manifested more and more clearly. The sample holder vibration accompanying the scanning process proved useful in revealing important details of the mechanisms underlying the impact of laser pulse radiation on the structure of irradiated films. Changes in film properties began to evolve in the volume of the films, and then they continued in surface morphological changes. To describe the observed processes, it was necessary to employ the whole complex of available experimental methods, each method, as a rule, allowing characterisation of a limited number (one or two) of the changing properties of the objects under study.

For instance, optical microscopy (Fig. 17 c) was sensitive to variations of optical parameters of the heterolayers under laser beam, manifested in color changes. This was an indication of the beginning of modification of material properties in some layers inside the coating. Those processes preceded the changes of the thickness and surface relief of the coating. SEM was effective only when studying surface morphology modifications (cp. Figs. 17 b, d, e, f and g). Besides, it has limited capabilities in height measurements of many relief details. However, when combined, the two methods were capable of revealing a complete picture of the dynamics of fs PLA induced changes in investigated multilayer structures on increasing the laser pulse energy.

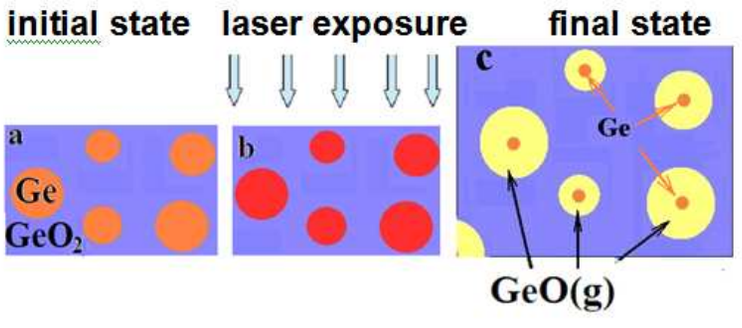

Figure 18. Schematic illustrating the process of transformation of a GeO_2<Ge-NCs> heterolayer in nanofoam-like glassy GeO_2 in a film structure subjected to fs laser annealing: **a** - initial heterolayer structure; **b** - heating of Ge-nanoclusters by fs laser pulses, which initiates the formation of GeO(gas) around these clusters; **c** - final structure of nanofoam-like glassy GeO_2.

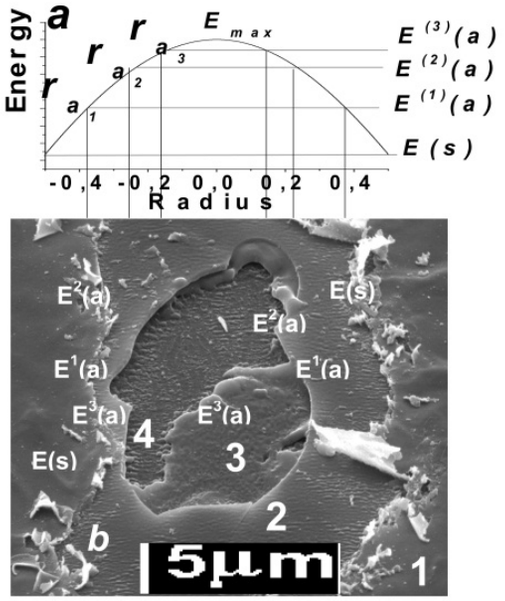

Figure 19. The simultaneous laser damage of two tiers of the multilayer system in Fig. 17 g during fs PLA (SEM image): **a** - radial Gaussian distribution of energy inside the laser beam; **b** - $E^{(1)}(a)$, $E^{(2)}(a)$, $E^{(3)}(a)$ - threshold energies for laser damage: (1) - in the top tier of the multilayer film system, (2) and (3) - in a thick SiO_2 layer and in a thick GeO_2<Ge-NCs> heterolayer of the middle top, respectively; $2r_{a1}$, $2r_{a2}$, $2r_{a3}$ - width of damaged areas in the respective layers of the system; $E(s)$ - threshold energy for the onset of the foaming process in thin GeO_2<Ge-NCs> heterolayers of the top tier of the multi-layer film system.

The experiment revealed some interesting features of the nanofoam formation process. First of all, the process was indeed implemented. The latter was indirectly proved by several methods of structural analysis. For instance, at an early stage of the process a wavy relief not violating the continuity of the multilayer coating emerged on the coating surface. The formation of this relief was registered by optical microscopy and SEM (Figs. 17 c and d). With increasing the laser pulse energy, the top tier in the coating starts destructing, and the smooth thick SiO_2 layer of the middle tier stands out. Then, the top tier of the coating detaches from the lower tier, tears and rolles, with all its thin layers becoming laminated (see Figs. 17 f and 19 b). This is the first stage of the laser damage of the whole multilayer system. Further on, the process laser damage develops involving more and more layers (Fig. 17 f and g and Fig 19 b), the boundaries of destructed zones in each layer spreading from the centerline of the laser treated path on the sample surface with growth of laser pulse energy. The ablated zone (band) in each layer is always wider than that in the lower layer. Therefore, SEM images allow observation of the structure and morphology of the uncovered surface of any exposed coating layer down to the Si-substrate surface.

Ultra-short laser pulses of the investigated heterostructures cause structural rearrangements and chemical reactions as: films shrinkage, GeO(solid) layers decay on reaction (3), growth of Ge-nanoparticles in the heterolayer and their crystallisation, chemical reactions of GeO_2 matrix of heterolayers with cap layers on their interface, possible crystallisation of GeO_2 glass around Ge-nanoparticles and reaction of GeO vapour formation from GeO_2<Ge-NCs>

heterolayer components, also ablation — explosive damage of films and substrates (Korte et al., 1999). Many of these processes are also expressed in radiation of GeO_2<Ge-NCs> heterolayers by fs Ti-Sapphire laser, just as in case of Kr excimer laser. But, as is seen from Fig. 17, the interaction character of fs laser radiation with the studied films and substrate was considerably different.

Results of using PLA and fs lasers for the studied film coatings showed that a number of the above-mentioned structural rearrangement processes and chemical reactions excite one by one with laser fluence growth. In general, to activate a new (i)-process, it is necessary to have laser fluence, absorbed by a film coatings square unit, exceeding the energy threshold of ($E^{(i)}$). Energy intervals among thresholds of different processes successively excited in films are usually so large that they can be definitely separated from each other. Therefore, the processes observed in multi-layer systems could be divided into two main groups. The first one consists of almost all the processes from the presented list, which proceed in the volume and interfaces of each of a multi-system's layers independently from processes in its other layers. Ablation processes belong to the second group as they, proceeding in one of a multi-system's layers, as a rule, determine all other processes in its lower layers.

4.2.3. Laser damage in multilayer coatings

In investigated heterostructures, ultra-short laser pulses induce various structural rearrangements and chemical reactions such as film shrinkage, decomposition of GeO(solid) layers according to reaction (3), growth of Ge-nanoparticles followed with their crystallisation in the heterolayer, chemical reactions of the GeO_2 matrix with the cap layers in the interfacial region, possible crystallisation of GeO_2 glass around Ge-nanoparticles and reaction (4) of GeO vapor formation from GeO_2<Ge-NCs> heterolayer components, and also ablation and explosive laser damage of the films and substrates (Korte et al., 1999). Many of these processes are manifested in GeO_2<Ge-NCs> heterolayers irradiated with fs Ti-Sapphire laser in a similar way like in the case of Kr excimer laser. However, as it is seen from Fig. 17, the interaction of fs laser radiation with examined films and Si substrate was largely different.

Results of using ns and fs PLA for treating examined film coatings showed that a sequence of the above-mentioned structural rearrangement processes and chemical reactions gets initiated on increasing the laser fluence. In general, for activation of a new (i-th) process, it is required to reach a laser fluence absorbed by a film coatings in unit square in excess of the energy threshold for the process ($E^{(i)}$). The energy intervals between the thresholds of the various processes successively initiated in the films are usually so large that they can be definitely separated from each other. Therefore, the processes observed in our multilayer systems could be divided into two main groups. The first group consists of almost all the processes from the above process list, which proceed in the bulk and interfacial regions of each of the involved layers independently of the processes proceeding in other layers. Ablation and laser damage processes belong to the second group as they, proceeding in one of the layers, as a rule, govern the processes proceeding in lower layers.

Successive onsets of structural-chemical modification processes of group I was observed in bilayer coatings given ns PLAs. In the case of fs PLA, successive (layer-by-layer) initiation of structural-chemical modification processes becomes distinctly pronounced during ablative destruction of multilayer coatings (see Fig. 19 b that shows a fragment of Fig. 17 f). It is seen that the laser pulse fluence absorbed by the multilayer coating is sufficiently high to exceed four energy threshold values, $E(s)$, $E^{(1)}(a)$, $E^{(2)}(a)$, and $E^{(3)}(a)$ (see Fig. 19 a). Three of the threshold energies are the thresholds for laser damage initiation in the two top tiers of the irradiated system (in the top tier and in the two layers of the middle tier, a thick SiO_2 layer and a GeO_2<Ge-NCs> heterolayer). The very first threshold energy is the non-ablative threshold $E(s)$ of the foaming process of three thin GeO_2<Ge-NCs> heterolayers in the top coating tier. The radial distribution of light energy in the laser beam obeys the Gauss law $E(r) = E_0 \exp(-2r^2 / r_0^2)$ (Korte et al., 1999) as shown in Fig. 19 a; therefore, destruction of the layered structures begins at the centerline of the laser treated path on the film surface when the pulse energy exceeds the necessary energy threshold of the top tier. $E^{(1)}(a)$ (see Fig. 19 b). If the pulse energy is sufficient to exceed the damage thresholds of the first, second and subsequent film, the laser damage will be initiated in all these layers simultaneously. Yet, ablative removal of the lower- coating material is impossible without a preliminary removal of the upper films. That is why, in most cases multilayer coatings are damaged successively, layer by layer. In this case the positions of the boundaries in destructed areas of each of the layers are determined by the radial energy distribution in the laser-beam cross section. Qualitatively, the theoretical expectation for this regularity is illustrated by Fig. 19 a. The experimental data of Fig. 17 f, g, and Fig. 19 b, in principle, do not disagree with the stated concept, although a multi-mode laser beam structure in real cases often distorts the strictly circular pattern of radial energy distribution in laser spots on irradiated surfaces. Thus, the processes activated in PLA-treated films experimentally revealed the real energy distribution round the laser-beam center.

The particular case under consideration is interesting in that respect that, apart from the propagation of the laser damage process into depth in a multilayer coating involving two types of films of different origin, here there was also a process that can be classed to intra-layer processes that can also proceed in layers covered by other films. This was the transformation process of fs PLA treated GeO_2<Ge-NCs> heterolayers into a nanofoam. The formation of nanofoam in germanate heterolayers was not hindered by thin SiO_2 layers that covered such heterolayers. Such SiO_2 layers were weakly heated by the laser beam, and they do not change their properties due to chemical and structural modifications. Simultaneously, this process progressed along the centerline of the fs laser treated path when the energy threshold of nanofoam formation E(s) was overcome during the fs PLA. If the laser fluence many times exceeded the threshold energy $E(s)$, then the top tier was immediately torn off from the middle tier as a homogeneous film according to the common explosive machanism of film damage. Here, the chemical nanofoam formation process did not have sufficient time to evolve in the GeO_2<Ge-NCs> heterolayers of this tier. Here, under fs laser irradiation the system of upper layers behaves as a solid film of homogeneous material. The thickness of this layer system at its edges along the line of damage rupture was almost no difference from the thickness of the whole layer on the substrate, and the

edges of the layer were like those of glassy films under brittle fracture. In other words, the edges mostly looked like broken line segments (Fig. 20 b, area 1), which were similar to the edges of thick SiO_2 layers after damage ruptures in the same multilayer coating (Fig. 20 b, areas 2 and 4).

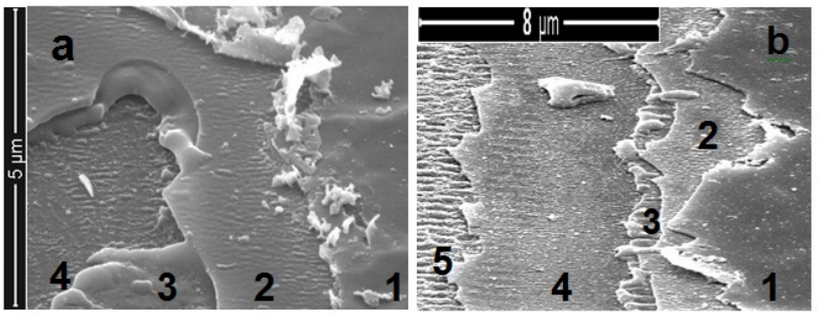

Figure 20. SEM image of layer-by-layer destruction processes in a multilayer structure exposed to laser radiation (**a** – E_{pulse} = 10 mJ , **b** – E_{pulse} = 13 mJ) : **1** - the top tier of thin layers, **2, 3** – the middle tier of thick layers (SiO_2 and nanofoamed GeO_2<Ge-NCs> heterolayer, respectively), **4, 5** – the bottom tier (lower SiO_2 layer and Si substrate, respectively.

However, laser damage took a different course if, under fs PLA, the laser fluence was only a little in excess of the threshold E(s) and the process of GeO_2<Ge-NCs> heterolayer foaming had sufficient time to develop. The thicknesses of those layers increased appreciably together with the thickness of the whole top tier in the multilayer coating; the top tier swelled and began to gradually tear off from the underlying SiO_2 layer. Then the areas of the top tier showing a most pronounced nanofoam formation suffered destruction accompanied by tearing off of its fragments (see Figs. 19 b and 20 a). Here, there are many thickened monolayer fragments of the top tier, exfoliated from the substrate incompletely and left in many areas over the edges of the layer along the centerline of the damage rupture zone. Those fragments roll in microtubes and laminate into very thin separate layers that constitute this tier (Figs. 19 b and 20 a).

During fs PLA, the nanofoam formation process of the thick GeO_2<Ge-NCs> heterolayer in the middle tier of the film coating proceeded in a different way than that in thin GeO_2<Ge-NCs> heterolayers of the top tier. The reason for this was that the thickness of GeO_2<Ge-NCs> heterolayer and its mass allowed it to accumulate more laser energy per unit volume. Moreover, a longer time was required for the damage process to cause removal of the thin film layers and the upper thick SiO_2 layer. Both factors allow the heterolayer to accumulate in its volume a considerable energy and considerably prolong the action of this energy transforming the heterolayer into nanofoam. Therefore, in all SEM images (Figs. 17 g, 19 b, 20 a and b) one can observe under the upper thick SiO_2 layer removed by laser damage a substance that looks like a liquid light foamy mass.

4.2.4. Some characteristic parameters of the nanofoam formation process

The thicknesses of the layers in the bottom and middle tiers as measured in SEM images were close to the values obtained in as-synthesized films. We could also conveniently

measure in the SEM images the thicknesses of the foam-like layers, which were found to 1,5-3 times exceed the initial thicknesses of the GeO_2<Ge-NCs> heterolayer. In some areal parts of the foam-like layers (where the layers became uncoated following the laser damage of the SiO_2 layer, Fig. 20), the foamy mass often increased, approximately by 2-4 times, the thickness of the GeO_2<Ge-NCs> heterolayer. During of the most foamed layer, some individual fragments of that layer were often explosively thrown up onto the SiO_2 layer. The thicknesses of those fragments were bigger than the three- or four-fold thickness of the SiO_2 layer.

As a rule, AFM data on the sizes of important relief features of the film coatings (Fig. 21) complied with the data obtained by other measuring techniques. Thus, AFM measurements proved that the top tier tears off from the underlying SiO_2 layer during laser damage ablation (Fig. 22). Besides, it is possible to determine the initial thickness (h) of the top tier (h ~50-60 nm) and the degree of its changes during fs PLA using the surface relief profile (Fig. 22 b) measured along the ***p***-line (Fig. 22 c). The obtained value for the thickness of the top tier (H) in the immediate vicinity of the damage rupture (Fig. 22 a, area 2) is five times greater than the initial layer thickness (h). But the value H is not only the result of transformation of the three GeO_2<Ge-NCs> heterolayers in the top tier into nanofoam. The laminating effect of the edges of the top-tier layers from the lower films in this area also contributed to the found value of H since after the tearing the free edges bent upwards.

The energy threshold of the foam formation process $E(s)$ in the thin GeO_2<Ge-NCs> heterolayers of the top tier during fs PLA was exceeded over the whole irradiated film surface (Figs. 21 and 22). Moreover, the rate of irradiation along the laser treated path (close to the line ***q*** in Fig. 22 a) varied periodically and at the points of maximum it reached the lower threshold energy for laser damage in this tier $E^{(1)}(a)$. In accordance with these periods, crests in swollen and buckled regions of the top tier formed. On the average, the separation between crests is 2,4 - 2,5 μm (line ***q*** in Fig. 22 a). There are zones in between the crests, where there was a minimal foaming of GeO_2<Ge-NCs> heterolayers. From the relief profile measured along the cutting line ***q*** (Fig. 22 d), we could determine the modulation frequency

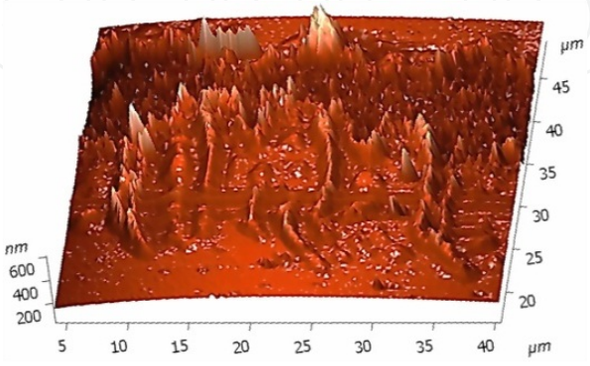

Figure 21. 3D AFM image of fs laser treated path on the multilayer surface shown in Fig. 17 e.

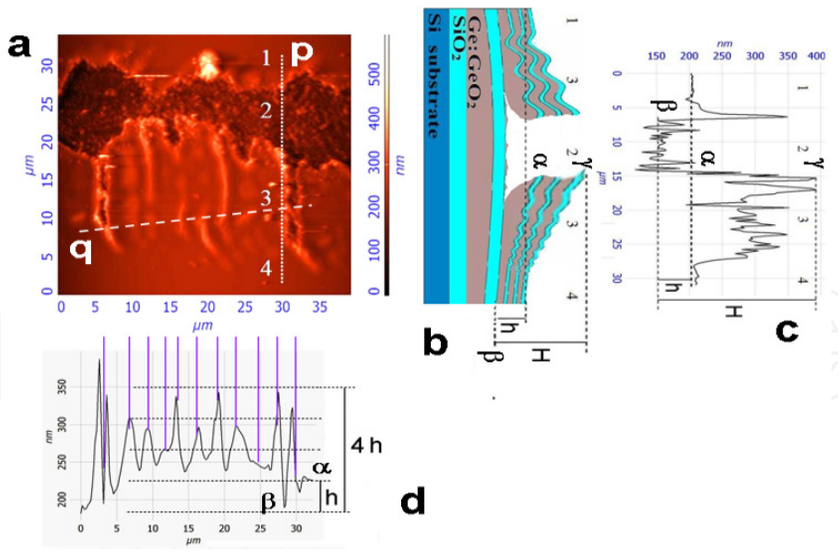

Figure 22. **a** - AFM image of the surface of the multilayer coating shown in Fig. 21: ***p*** and ***q*** - cutting lines of the sample surface across and along the fs laser treated path, respectively; **b** – schematic of the sample cross section along the line ***p*** drawn along the rupture edge of the the top tier of the coating with swelled films (**1** and **4** - areas with unchanged relief, **2** - laser damage zone of the top tier, **3** - zone of the maximum change in relief at the edge of rupturing film during its swelling; **c** - relief of the film coating along the line ***p***: ***α*** - the initial level of coating surface, ***β*** - surface of the upper thick SiO_2 layer, ***γ*** - the highest level of coating relief changes, **d** - relief of the film coating along the line ***q*.**

of laser beam energy connected with the sample vibration. An analysis of this relief in the described fs PLA conditions showed that, at this modulation frequency of laser irradiation, its energy changes within the interval between the threshold energies of the two processes $E^{(1)}(a)$ and E(s) during the period of ~ 0,025 sec. The thickness of GeO_2<Ge-NCs> heterolayers may increase 3-4 times for the time equal to half the period.

As a result, the vibration experiment revealed: (i) a low threshold energy *E(s)* of the process; (*ii*) a high capability of GeO_2<Ge-NCs> heterolayers to increase of their volume (by 3-5 times) during transformation into nanofoam material; (*iii*) high dynamic characteristics of the nanofoam formation process during increase of fs laser pulse energy.

Micro-Raman spectra of fs laser treated GeO_2<Ge-NCs>heterolayers (Fig. 23) produce another evidence of their transformation into a nanofoam-like material. For simplification of the analysis, the spectra were registered in GeO_2<Ge-NCs> heterolayers deposited onto a Si substrate protected by a 25-nm thick SiN_xO_y cap layer (the effect due to ns PLA was also studied on this sample). The effect due to laser fluence value exciting the nanofoam formation process in local regions of the GeO_2<Ge-NCs>/SiN_xO_y bilayer system is shown in Fig. 23. In Fig. 23 a, in spectrum 1, which corresponds to non-irradiated film at point 1 (Fig. 23 e), only a broad Raman band due to light scattering by transversal optical phonons of α-Ge is shown, like in the case of ns laser treatment of this film system (Fig. 12).

As it can be judged from the weak scattering peak of the beam of the exciting Ar^+ laser of Raman spectrometer due to the Si-substrate lattice (scattering band in the region of 520 cm^{-1}), the film system was little transparent to this beam. Raman spectra 2 and 3 in Fig.

23 a were obtained at two closely located points (2 and 3) on one of the lines treated by the fs laser beam (Fig. 23 d and e, respectively). Yet, because of heterogeneity of the radial energy distribution in the beam, intensive formation of nanofoam mass from the GeO_2<Ge-NCs> heterolayer proceeded at both points of this line during PLA. At point 3, the film coating was at an early stage of destruction, still remaining almost intact, whereas at point 2, damage was well activated. The latter is evident from the intensity of the Raman peaks of Ar^+ laser beam due to Si-substrate lattice (in the corresponding spectra); at point 2 the film practically does not hinder the Ar^+ laser beam to reach the substrate. In other words, at points 2 and 3 we observe an early and the final stage of the destruction process of the foamed layer. Nonetheless, despite the possibility of mixing up film fragments belonging to different areal parts of the film, Ge-nanocrystal sizes were not large, ~2,3 – 3,1 nm as calculated by model (1) and ~3,1 - 4,1 as calculated by model (2). At point 4 in Fig. 23 c the fs laser energy was slightly lower than that at points 2 and 3. Therefore, the film foamed without and violation of its continuity. Ge-NCs of the least diameter ~1,0 (model (1)) and 1,4 nm (model (2)) were found here (spectrum 4 in Fig. 23 a).

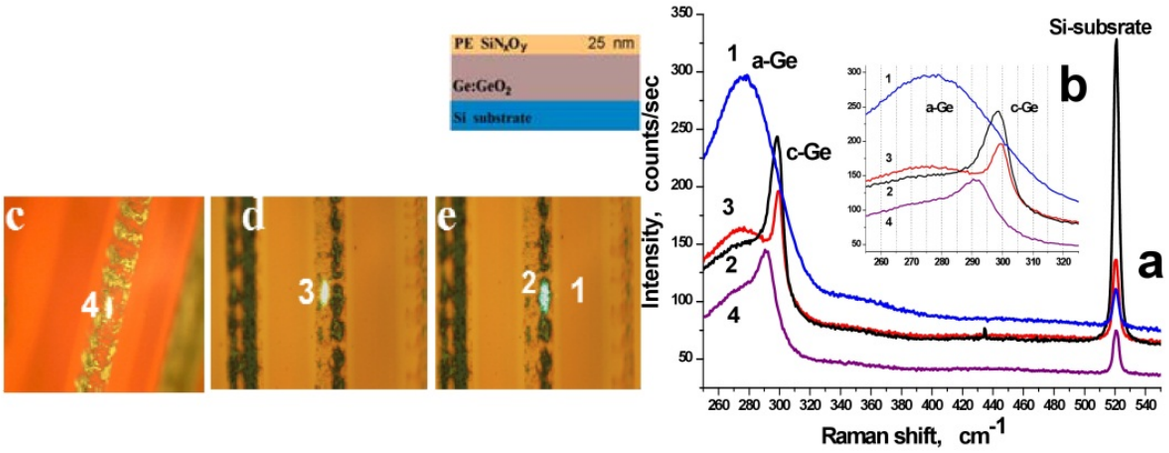

Figure 23. **a, b** - Raman spectra and **c, d, e** - photos of GeO_2<Ge-NCs> heterolayers transformed to nanofoam under a SiN_xO_y cap layer on the Si substrate: **1** – non-irradiated films; **2** - strong laser damage of the films; **3** - laser damage at an early stage; **4** - the formation of foam without destruction of the cap layer.

Thus, the both main features which are to accompany the formation of nanofoam from GeO_2<Ge-NCs> heterolayers during their fs laser pulse treatments were observed in the experiment. Direct images of the studied material are supposed to be obtained with HR TEM, but additional information about the properties of the nanofoam was also obtained with the SEM method. Characterizing the most impressive effects produced in GeO(solid) films and GeO_2<Ge-NCs> heterolayers by fs PLA, we would like to note that, here, the same structural and chemical modification processes like those in ns PLA treated samples proceed both consequently and in parallel in the material; those process include: decomposition of the metastable solid germanium monoxide atomic network with its transformation into the atomic network of glassy GeO_2 oversaturated with Ge atoms; clusterization of released germanium into amorphous nanoparticles; and growth and crystallisation of α-Ge nanoparticles. The effect of film transparency increase is also common for both kinds of laser

treatments during crystallisation of α-Ge nanoparticles in the film bulk. On the other hand, the main difference between the effects due to UV ns and IR fs PLAs on GeO_2<Ge-NCs> heterolayers consists in that UV ns laser radiation leads to a considerable shrinkage of the material, whereas IR fs radiation leads to transformation of the whole irradiated heterolayer material into a very loose foam containing nanocavities separated with ultra-thin glassy GeO_2 barriers. An SEM image of the nanofoam obtained by fs PLA of GeO_2<Ge-NCs> heterolayers unprotected by cap layers (Fig. 24 d) confirms such a microstructure of the obtained material.

Another remarkable feature is that the ablation and laser damage of the multilayer system proceeding together with the formation of nanofoam in GeO_2<Ge-NCs> heterolayers (Fig. 17 and 23) are processes highly sensitive to even small variations in the fs laser fluence distributed over the surface of the multilayer. On the contrary, the shrinkage process of the same multilayer system (illustrated by Figs. 7 c and 10) under ns pulsed laser radiation, even at the highest energies, demonstrates high uniformity of the irradiated coating surface. In GeO_2<Ge-NCs>/Si_xN_yO bilayer films consisting predominantly of GeO_2<Ge-NCs>, no ablation or laser damage effects were observed in the examined ranges of heterolayer thicknesses and laser fluences.

The causes for this difference may be somehow related with the fact that the shrinkage of heterolayer thickness is a process that proceeds at a rate ten times slower in comparison with the nanofoam formation process. The volume of a foaming heterolayer normally increases by a few hundred per cent, whereas the maximum shrinkage of film thickness (in the case of ns laser treatment) does not exceed 40 per cent. It is possible that during the latter relatively slow process local temperature non-uniformities get smoothed over the film. In other words, temperature and stress gradients have enough time to disappear from the film. Another cause may be related to the fact that the mechanisms of laser radiation absorption by the material in the two cases are very different. In GeO_2<Ge-NCs> heterolayers, the ultraviolet radiation emitted by ns pulsed laser is readily absorbed not only in Ge NCs, but also in the glassy GeO_2 matrix. As a result, the matrix, absorbing the main part of the incident light, undergoes quick heating. Ge NCs absorb less energy of light pulses in the heterolayer as they occupy only about 30% of its volume. Microscopic regions that do not absorb laser radiation are absent from heterolayer, making the distribution of absorbed heat in the film volume less inhomogeneous. If the average temperature in heterolayer does not exceed the energy threshold for GeO(gas) formation due to reaction (4) at the interface between the GeO_2 matrix and Ge-nanoclusters, the heterolayer shrinkage process will mainly depend on the matrix viscosity. The temperature of the film defines the film material viscosity. Then, it can be anticipated that the shrinkage process in the film will most likely proceed similarly to the shrinkage during traditional anneals of ordinary CVD SiO_2 and Si_3N_4 films (as described in Section 3.3). Due to this shrinkage mechanism, much of the internal lateral stresses turn out to be reduced by viscous flow of the material. The lower the viscosity the more readily the film shrinking process proceeds.

In the case of fs laser treatments of GeO_2<Ge-NCs> heterolayer, radiation will be absorbed only in Ge-nanoclusters. As a result, the distribution of the heat absorbed in the heterolayer

should be much less homogeneous in comparison with the case of ns laser pulses. Temperature gradients in heterolayer, which are created by fs laser pulses between the cold glass and the heated Ge-nanoclusters can be expected quite high because all the energy of the light absorbed in the heterolayer is transferred into the heterolayer bulk only through the boundaries of Ge-NCs with the glass matrix. Thus, in this system only a small part of the glass directly bordering on heated Ge-nanoclusters can be quickly heated to high temperatures, while the rest part of the glass matrix will undergo heating at a much slower rate. Such a state of the heterogeneous material will be characterised by abrupt spatial variations of temperature and compressive stress over the volume of the heterolayer occurring over distances comparable with Ge-NC sizes. In particular, effects associated with thermal expansion coefficients of GeO_2 glass and Ge-NCs, as well as with the formation of high-pressure GeO(gas) bubbles around Ge-clusters, will facilitate smoothening of internal stress inhomogeneity. The impact action of fs laser pulses stimulates rapid evolution of the latter state of the material in heterolayer.

4.3. Prospects for use of GeO_2<Ge-NCs> heterolayers in medicine and laser lithography

High sensitivity to laser irradiation readily activating the evaporation reaction of GeO(solid) films and GeO_2<Ge-NCs> heterolayers proceeding with the formation of volatile germanium monoxide is an interesting prerequisite for using such films as a nanoresist in laser lithography. Therefore, some experiments were carried out to evaluate the potential offered by the examined films in this field. In our study, GeO(solid) films and GeO_2<Ge-NCs> heterolayers not covered with cap-layers were used. Such films and heterolayers were deposited onto pure Si substrates or onto SiO_2 layers grown by CVD on Si. Then, the films were subjected to fs Ti-Sapphire laser PLA in the same way like in previously described experiments with multilayer coatings, except for the laser beam was focused in ~1-μm diameter spot and the pulse energy falling onto the sample was decreased with the help of optical filters. The maximum laser-beam energy (E_{max}) was chosen to exceed the threshold energy ($E^{(1)}$(nfoam)) of the foam formation process in the heterolayer yet it was lower than the threshold energy $E^{(2)}(evap)$ of the evaporation reaction of the film GeO (Fig. 24 a). Such a beam was used to scan the surface of a heterolayer on a Si substrate covered with a SiO_2 film. The sample was mounted on an optical bench vibrating in the lateral plane and vertically within 1 - 1,5 μm. In the sample vertical vibration, the laser beam focus was on the film at one turning point 1 of the oscillation period, and the focus raised over the film surface during the reverse motion of the optical bench. In the first case, the beam had a minimal diameter on the sample ($2r_{o1} \sim \lambda$) and a maximal energy value (E'_{max}) which was higher than the evaporation threshold of the film $E^{(2)}$(evap) and its foaming threshold $E^{(1)}$(nfoam) (i.e. $E'_{max} > E^{(2)}(evap) > E^{(1)}(nfoam)$). The defocused beam in point 2 had the biggest diameter $2r_{o2} > 2r_{o1}$ and a minimal value of the energy maximum (i.e. $E''_{max} < E^{(1)}(nfoam)$ and $E^{(2)}(evap)$).

The results of such scanning of the used GeO_2<Ge-NCs> heterolayer ~ 60-80 nm thick with a vibrating beam spot are shown in Fig. 24 b and c. The track width periodically varies due to

pulse energy modulation by the sample vertical vibration. No changes in film material properties were observed within the laser treated path at point 2 (Fig. 24 b) as the laser pulse energy on the layer surface was minimal here. The foam formation process is initiated in the heterolayer when the laser pulse energy on its surface grows in magnitude along the laser treated path due to light beam narrowing. The reaction zone eventually broadens up, and the film thickness at the beam centre increases by ~2 - 3 times. At the moment when the rate of the process is maximal, the heterolayer evaporation energy becomes exceeded (point 1 in Fig. 24 b) as the energy E'_{max} in the experiment was a little higher than $E^{(2)}(evap)$. Evaporation begins at the beam centre, analogously to the reaction of foam formation. The stretch of laser treated path over which this reaction proceeds is not long as the distance between the focusing lens and the sample changed due to vibrations simultaneously with the lateral shift of the beam over its trajectory. So, the beam on the sample surface again becomes defocused, and the nanofoam evaporation process ceases. In this case, the width of the cavities (~11-50 nm) formed by the beam in the foamed layer is quite appreciable (Fig. 24 b and c). This result attracts attention, as in geometric optics a spot having a diameter less than ~$\lambda/2$ is considered to be the diffraction limit of beam focusing, and the traces of its effect for photoresist should be close to this size considered as the physical limit for laser lithography line width. Through-holes shaped as round dots or prolonged windows, whose transversal sizes were ten times larger than the expected limit were obtained in our experiments with laser radiation wavelength λ=800 nm.

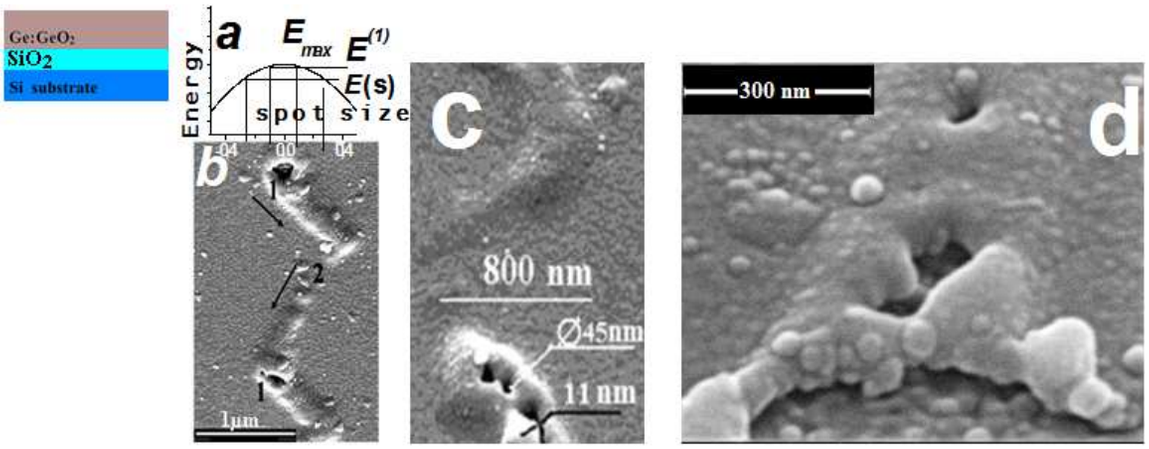

Figure 24. SEM images of the local formation of nanofoam in a GeO_2<Ge-NCs> heterolayer without a cap layer after fs laser irradiation (beam diameter ~ 1 μm;): **a** - radial Gaussian distribution of light energy in the laser beam; $E(s)$ and $E^{(1)}(evap)$ are the threshold energies for foaming and evaporation of the heterolayer material, respectively; **b** and **c** - focused beam treated paths on the heterolayer surface during horizontal and vertical microvibrations of the optical bench; **d** – nanofoam.

The mechanism behind the laser beam effect on the GeO_2<Ge-NCs> heterolayer has not been adequately understood. Possible explanations of the sharp narrowing of the high-flux zone in the laser beam section on the film surface were considered, including intermode interference of light rays inside the laser beam and the effect of two-photon absorption of light by the film in areas with high degree of radiation power localization on the film surface.

Note that in this experiment no additional measures were taken to stabilize the irradiation conditions of GeO(solid) films and GeO_2<Ge-NCs> heterolayers used as a resist in laser lithography. We, however, believe that further considerable progress can be achieved along this line of research. However, in this way, even at the technological level available to us it was possible to fabricate some simple optical devices. In particular, the evaporation process of GeO_2<Ge-NCs> heterolayers by fs laser beam focused to a 1-μm diameter spot was used to fabricate prototypes of diffraction gratings (see Fig. 25). GeO_2<Ge-NCs> heterolayers 25 – 300 nm thick were scanned with laser beam at a speed 100 μm/s and frequency 1 kHz in the air. For the chosen heterolayer thickness, laser pulse energy was matched to slightly exceed the film evaporation energy threshold. The results showed that, under such conditions, it was possible to prepare diffraction gratings with line density up to 1000 lines per 1 mm.

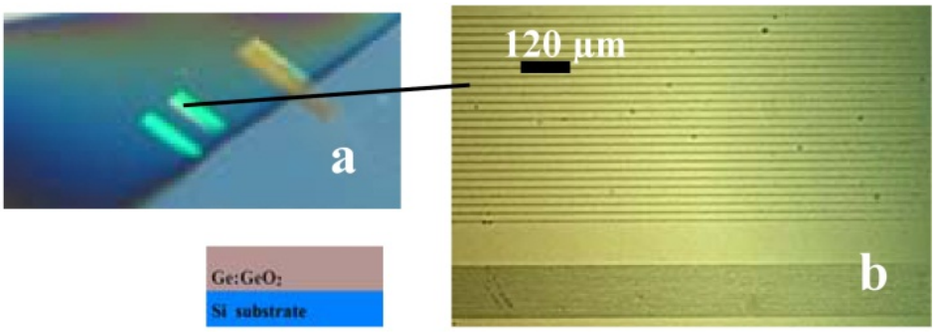

Figure 25. Diffraction of white light (**a**) on a set of lines in GeO_2<Ge-NCs> heterolayer on Si-substrate formed by a dry laser lithography (**b**) (optical microscopy photos).

As is seen, the main idea behind this method is that laser irradiation can be used to heat Ge-nanoparticles incorporated in a continuous medium. This idea differs little from the idea of using such Ge-nanoparticles in nanofoam formation from GeO_2<Ge-NCs> heterolayers. Therefore, we tried to employ Ge-nanoparticles in destructing malignant tumors. First, it is necessary to become able to prepare germanium particle based colloid solutions. It may be not so difficult a problem. A GeO_2 matrix with embedded Ge-nanoclusters is readily soluble in water or aqueous solutions of various active organic or inorganic chemicals. It is easy to find among the various chemicals those inert to germanium. Using such solutions, we can transfer Ge-nanoclusters from GeO_2<Ge-NCs> heterolayers into a suitable colloidal solution. This is one possible way towards solving the problem. Another strategy here is based on the ability of germanium to relatively slowly dissolve not only in liquid aggressive media, both acid and alkaline, but also in water. The solving proceeds in two stages: (*i*) oxidation of Ge-nanoparticle surface to GeO_2; (*ii*) dissolution of the oxide in a solvent. In some time, the colloidal germanium particles introduced in human organism will become completely dissolved to be removed from it in a natural way.

Another possible application of the results described above may be the use of Ge-NCs in medicine to suppress malevolent tumour formation. A method of tissue destruction in malignant tumours is widely known; it employs injection of colloidal solutions containing Ag-NCs with average diameter ~ 5-7 nm into tumor (Tyurnina et al., 2011). Ag-NCs spread over the tumour body and penetrate some part of its cells. Then the tumour is to be exposed

to a laser beam which burns out the soft tumour tissues to a big depth due to heating of Ag-NCs.

5. Conclusions

The main aim of this paper was to describe the technological potential of pulsed laser treatments in modification of properties of film heterosystems involving germanium oxide layers with embedded Ge-nanoparticles. The goal of the study was the development of a general concept of physical-chemical mechanisms underlying such processes, i.e. suggestion 1 of a physical picture, or materials-science concept with analysis of reasons and outcomes, rather than the search for particular processes ensuring required modifications together with identification of appropriate technological conditions.

The general scientific aspect of the research involved two tasks. One of the tasks concerned fundamental problems in studying effects and processes connected with the input of large amounts of energy into small volumes of a solid, i.e. with the behavior of substance absorbing ultra-short laser pulses and subsequent relaxation of excitations in the solid body and surrounding medium. The second task was investigation of changes of structura chemical, physical and electrical properties of thin films under such treatments. New was the study of structural changes under pulsed laser treatments in multi-layer insulating coatings containing the films with a high concentration of QDs in the form of semiconductor nanoparticles. More specifically, we examined only one kind of such films, formed by germanium oxide layers (GeO and GeO_2) with embedded Ge-QDs.

A characteristic feature of both kinds of the effects due to PLA on studied multilayer coatings was that ultra-short laser pulses locally absorbed in small volumes of some cubic microns led to relaxation of this energy in volumes many times bigger than the sizes of the absorption zone while the duration of the dissipation process of absorbed energy lasted for a time that exceeded the laser pulse duration by many orders.

If it were not so, then we could not detect in the irradiated films indications of such slow and very large-scaled processes as films densification (by some ten percents), diffusion (up to 30% of the film material mass at distances of some hundred nm), rearrangement of the atomic network of the material from one kind into another, and ablation. In other words, all these modification processes of the material structure show that part of the material absorbed laser pulse energy from subsystems with superfast processes (subsystems of electromagnetic radiation, electron and phonon subsystems) spread into the subsystem of lattice processes. The latter subsystem has longest excitation relaxation times during chemical and structural rearrangement processes. Those long relaxation times are due to the fact that these rearrangements are collective, involving many atoms. Within such ideas, it can be speculated that, increasing the laser power, we will enter the conditions under which part of the energy absorbed by the solid will become sufficient for excitation of shock waves in the sample. These waves will begin to mechanically destroy the sample into fragments scattering around. This effect is called ablation.

An analysis of experimental data showed that, under PLA, layered films capable of good absorption of laser radiation play a big role in laser pulse energy accumulation. In the present case, those were GeO(solid) layers, GeO_2<Ge-NCs> heterolayers, and also the silicon substrate. All of the layers conveyed the absorbed energy either in heat or in structural chemical modification processes. The latter is clearly seen in Fig. 17 e and f, where the ablation process in the treated materials begins as the formation of ripples well before the thick SiO_2 layers covering the materials are exploded. In cases where thick GeO_2<Ge-NCs> heterolayers were absent from the multilayer coatings or when the silicon substrate absorbing radiation was replaced with transparent glass, increased threshold energies for all the processes activated in the multilayer system under PLA were observed.

From these standpoints, one can suggest an explanation to the opposite results obtained for two kinds of fs and ns PLA of GeO_2<Ge-NCs> heterostructures when, in one case, we had the formation process of super-loose nanofoam-type structure and, in the other case, a layer of a material having a very high density. In fs laser treated GeO_2<Ge-NCs> heterolayers, the laser pulses, 30 fs long, follow at 1-ms intervals, with the predominant part of their energy being absorbed by Ge-NCs. Suppose that this energy has enough time to completely dissipate for less than 1 msec. Then, strictly speaking, an act of energy absorption by this Ge-nanoparticle is no different from a similar act for the next pulse. This means that, in each of the pulses, identical portions of nanocluster-absorbed energy will produce identical amounts of gaseous monoxide at the boundary of the Ge-nanocluster with the surrounding GeO_2 glassy matrix. But to return the system to its strictly initial state till the coming of the next pulse, gas GeO formed around the Ge-nanoparticle should again transforms into initial solid components of Ge and glassy GeO_2. Otherwise, the absorption act of the second laser pulse by Ge-nanoparticle will not be strictly identical to the first one. It means that the whole nanofoam formation process will be confined to the process with a periodical alternation of two phases – one during which minimal setting nanofoam quantities form for less than 1 ms and the phase during which they disappear so quickly.

A different result was obtained in the experiment: nanofoam formation turned a stable and irreversible process. Logically, henceforth it follows that, in a series of fs laser pulses, each is absorbed by the GeO_2<Ge-NCs> heterolayer in the conditions different from the absorption of the previous ones. So, the effect of their impact should be considered not as a set of discreet and disconnected flashes, but as some continuous process proceeding during the duration of a whole pulse series. In fact, it shows that the complete time of energy relaxation by GeO_2<Ge-NCs> heterolayer absorbed from a separate pulse is longer than the intervals between them. Therefore, accumulation of some energy part of each pulse proceeds in the heterolayer. This accumulation integrates the whole series of discreet flashes in a continuous action that consists of three stages – the initial stage, the stage of stationary mode and the final stage that proceeds upon the completion of radiation. During PLA of GeO_2<Ge-NCs> heterolayer with ns laser, the time spans between laser pulses are so big that one cannot say about the thing that their effect is connected with part of their energy accumulation by GeO_2<Ge-NCs> heterolayer from pulse to pulse. Besides, GeO_2 matrix considerably absorbs ns laser pulse energy in the

GeO_2<Ge-NCs> heterolayer. Accordingly, the part of the pulse energy absorbed by Ge-nanoparticles considerably decreases and, along with it, their heating rate also decreases. If the speed of Ge-NCs heating in the heterolayer is lower than that of GeO_2 matrix, then the matrix will be cool down close to the border between these two heterolayer components, as it spends part of its heat for heating colder Ge-NCs. In the rest part of the glassy GeO_2 matrix, with the growing temperature, the decay processes of atomic net remaining parts of metastable GeO(solid) and its shrinkage by lowering atomic GeO_2 net defectiveness proceed. The latter of these processes is usually accompanied by a viscosity increase in glasses and that is to cause threshold energy growth of a beginning of foam formation in the GeO_2<Ge-NCs> heterolayer. Thus, the totality of all the described factors impairs, in this case, GeO_2<Ge-NCs> heterolayers transformation into a nanofoam-like matter under their ns laser pulse radiation under the conditions used in our experiments.

At the end of this research work, we emphasise one more time that it is difficult so far to find out of a multitude of film coatings and materials this or that way involved in microelectronics such their kinds that would characterised by so high capability to properties and structure modification and absolutely all the properties as germanium oxide layers. Although, as we believe, silicon oxide-based films are the most chemically close to them. These materials also have the capability to different modification forms and radical changes of many physicochemical properties. Particularly, in our viewpoint, SiO_2 layers transformation into nanofoam-like material may be one of the most interesting out of modifications similar to those of germanium oxides. It is not excluded that it will be realised by the way analogous to the used one for nanofoam formation from glassy GeO_2.

The authors hope that the possibilities demonstrated in our paper for germanium oxide layers modification assisted with laser treatments will attract attention of material scientists in the field of film coatings used in nano- and optoelectronics and also of researchers engaged in applied trends of nanotechnology.

Author details

Evgenii Gorokhov, Kseniya Astankova, Alexander Komonov and Arseniy Kuznetsov
Institute of Semiconductor Physics of SB RAS, Russia
Laser Zentrum Hannover, Germany

Acknowledgement

This investigation was supported by the Russian Fundation for Basic Research (projects Nos. 07-08-00438 and 10-07-00537). E.B. Gorokhov is grateful to Universite' de Nancy (France) and Laser Zentrum Hannover (Germany) for a visit grant. Also, the authors thank their colleagues for assistance in work: Dr. D.V. Marin, Dr. T.A. Gavrilova, Dr. V.A. Volodin, M. Slabuka, Prof. Boris Chichkov from Laser Zentrum Hannover (Germany), Prof. M. Vergnat from Institute Jean Lamaur and l'Universite' de Lorraine for their help in studying GeO(solid) films and Prof. A.V. Latyshev for financial support.

6. References

Ahmanov, S.A.; Yemel'yanov, V.I.; Koroteev, N.I. Seminogov, V.N. (1985). The Impact of High-Power Laser Irradiation on the Surface of Semiconductors and Metals: Nonlinear Optical Effects and Nonlinear Optical Diagnostics. *Advances in Physical Sciences,* Vol. 147, No. 4, pp. 675-745

Appen, A.A. (1974). Chemistry of Glass. 2nd Edition. *Publ.: Khimiya, Leningrad (In Russian).*

Ardyanian, M.; Rinnert, H.; Devaux, X. & Vergnat, M. (2006). Structure and Photoluminescence Properties of Evaporated GeO_x Thin Films. *Appl. Phys. Lett.,* Vol.89, pp. 011902-1-3

Ashitkov, S.I.; Ovchinnikov, A.V. & Agranat, M.B. (2004). Recombination of an Electron-hole Plasma in Silicon Under the Action of Femtosecond Laser Pulses. *JETP Letters,* Vol.79, No 11, pp. 529-531

Bok, J. (1981). Effect of electron-hole pairs on the melting of silicon. *Phys. Lett.*, Vol. 84 A., No. 8., pp. 448-450

Chong, T.C.; Hong, M.H. & Shi, L.P. (2010) Laser Precision Engineering: From Microfabrication to Nanoprocessing. *Laser&Photon. Rev.,* Vol.4, No 1, pp. 123-143

Dvurechenskiy, A.V.; Kachurin, G.A.; Nidaev, N.V.; Smirnov, L.S. (1982). Pulsed Annealing of Semiconductor Materials. *Publ.: Nauka, Novosibirsk (In Russian).*

Ekimov, A.I. & Onushchenko, A.A. (1981). Quantum-Size Effect in Three-dimensional Microscopic Semiconductor Crystals. *JETP Lett.,* Vol.34, No.6, pp. 345-348

Filipovich, V.N. (1978). The Theory of Self-Diffusion of Oxygen in Glassy SiO_2, GeO_2. *Glass Physics and Chemistry.* Vol.4, No.1, pp. 22-30

Gallas, B.; Kao, C.-C.; Fisson, S.; Vuye, G.; Rivory, J.; Bernard, Y. & Belouet, C. (2002). Laser Annealing of SiO_x Thin Films. *Appl. Surf. Science,*Vol. 185, pp. 317–320

Gorokhov, E.B.; Kosulina, I.G.; Pokrovskaya, S.V. & Neizvestny, I.G. (1987). Mechanical and Electrical Properties of the Double-layer Film System GeO_2-Si_3N_4 on Ge. *Phys. Stat. Sol. (a),* Vol.101, pp. 451-462

Gorokhov, E.B.; Noskov, A.G.; Sokolova, G.A.; Stenin, S.I.; Trukhanov, E.M (1982). Mechanical Stability of Pyrolytic Silicon Dioxide Films. *Physics, Chemistry and Mechanics of Surfaces (In Russian – Surface),* No.2, pp.25-33

Gorokhov, E.B.; Prinz, V.Y.; Noskov, A.G. & Gavrilova, T.A. (1998). A Novel Nanolithographic Concept Using Crack-assisted Patterning and Self Alignment Technology. *J. Electrochem. Soc.,* Vol.145, No.6, pp. 2120-2131

Gorokhov, E.B. (2005). *Evaporation and Crystallisation Processes in Germanium Oxide Films on Germanium*. PhD thesis, SB RAS, Novosibirsk, Russia

Gorokhov, E.B.; Volodin, V.A.; Kuznetsov A.I.; Chichkov B.N.; Astankova, K.N. & Azarov, I.A. (2011). Laser Treatment of the Heterolayers "GeO_2:Ge-QDs". *Proc. of SPIE*, Vol.7994, pp. 79940W-10

Hrubesh, L.W. & Poco, J.F. (1995). Thin Aerogel Films for Optical, Thermal, Acoustic and Electronic Applications. *Journal of Non-Crystalline Solids,* Vol. 188, pp. 46-53

Jambois, O.; Rinnert, H.; Devaux, X. & Vergnat M. (2006). Influence of the Annealing Treatments on the Luminescence Properties of SiO/SiO_2 Multilayers. *J. Appl. Phys.*, Vol.100, pp. 123504-6

Jolly, M. & Latimer, W.M. (1952). The Equilibrium Ge(s) + GeO_2(s) = 2GeO(gas). The Heat of Formation of Germanic Oxide. *J. Amer. Chem. Soc.*, Vol.74, No20, pp. 5757-5758

Juodkazis, S.; Mizeikis, V. & Misawa, H. (2009). Three-dimensional Microfabrication of Materials by Femtosecond Lasers for Photonics Applications. *J. Appl. Phys.*, Vol. 106. pp. 051101-1-14 Kachurin, G.A.; Pridachin, N.B.; Smirnov, L.S. (1975). Annealing of Radiation Defects by Pulsed Laser Irradiation. *Semiconductors,* Vol. 9, No. 7, pp. 1428-1429

Kamata, Y. (2008). High-k/Ge MOSFETs for Future Nanoelectronics. *Materials Today,* Vol.11, No.1-2, pp. 30-38, ISSN 1369-7021

Knoss, R.W. (2008). *Quantum Dots: Research, Technology and Applications,* Nova Science Publishers Inc., New York

Korchagina, T. T.; Gutakovsky, A. K.; Fedina, L. I.; Neklyudova, M. A. & Volodin, V. A. (2012). Crystallisation of Amorphous Si Nanoclusters in SiO_x Films Using Femtosecond Laser Pulse Annealings. *Journal of Nanoscience and Nanotechnology* (in print)

Korte, F.; Nolte, S.; Chichkov, B.N.; Bauer, T.; Kamlage, G.; Wagner, T.; Fallnich, C. & Welling H. (1999). Far-field and near-field Material Processing with Femtosecond Laser Pulses. *Appl. Phys. A.*, Vol. 69, pp. S7-S11

Marin, D.V.; Gorokhov, E.B.; Borisov, A.G. & Volodin, V.A. (2009). Ellipsometry of GeO_2 Films with Ge Nanoclusters: Influence of the Quantum-size Effect on Refractive Index. *Optics and Spectroscopy,* Vol.106, No3, pp. 436-440, ISSN 0030-400X

Marin, D.V.; Volodin, V.A.; Gorokhov, E.B.; Shcheglov, D.V.; Latyshev, A.V.; Vergnat, M.; Koch, J. & Chichkov, B.N. (2010). Modification of Germanium Nanoclusters in GeOx Films During Isochronous Furnace and Pulse Laser Annealing. *Technical Physics Letters,* Vol.36, No5, pp. 439-442

Martynenko, A.P.; Krikorov, V.S.; Strizhkov, B.V. & Marin, K.G. (1973). Physicochemical Properties of Silicon and Germanium Monoxide. *Inorganic materials*, Vol.9, No.9, pp. 1394-1399

Martsinovsky, G.A.; Shandybina, G.D.; Dement'eva, Yu.S.; Dyukin, R.V.; Zabotnov, S.V.; Golovan', L.A. & Kashkarov, P.K. (2009). Generation of Surface Electromagnetic Waves in Semiconductors Under the Action of Femtosecond Laser Pulses. *Semiconductors,* Vol.43, No10, pp. 1298-1304

Molinari, M.; Rinnert, H. & Vergnat, M. (2003). Visible Photoluminescence in Amorphous SiOx Thin Films Prepared by Silicon Evaporation Under a Molecular Oxygen Atmosphere. *Appl. Phys. Lett.,* Vol.82, No.22, pp. 3877-3879

Mueller, R.L. (1960). Chemical Characteristics of Polymer Glass-Forming Substances and the Nature of Glass Formation. Book: Proceedings of the Third All-Union Conference on the Glassy State. *Publ.: The USSR Academy of Sciences, Moscow and Leningrad.* Pp.61-71

Mueller, R.L. (1955). A Valence Theory of Viscosity and Fluidity for High-Melting Glass-Forming Materials in the Critical Temperature Range. *Journal of Applied Chemistry (Russian Journal of Applied Chemistry).* Vol.28, No.10, pp. 1077-1087

Nelin, G. & Nilsson, G. (1972). Phonon Density of States in Germanium at 80 K Measured by Neutron Spectrometry. *Phys. Rev. B*, Vol.5, pp. 3151-3160

Nemilov, S.V. (1978). The Nature of the Viscous Flow of Glasses with Frozen Structure and Some of the Consequences of Valence-Configuration Theory of Viscous Flow. *Glass Physics and Chemistry.* Vol.4, No.6, pp. 662-674

Nemilov, S.V. (1978). The Valence-Configuration Theory of Viscous Flow of Supercooled Glass-Forming Liquids and its Experimental Validation. *Glass Physics and Chemistry.* Vol.4, No.2, pp. 129-148

Ogden, J.S. & Ricks, M.J. (1970). Matrix Isolation Studies of Group IV Oxides. II. Infrared Spectra and Structures of GeO, Ge_2O_2, Ge_3O_3, and Ge_4O_4. *J. Chem. Phys.*, Vol.52, No1, pp. 352-357

Pliskin, W.A.; Lehman, H.S. (1965). Structural Evaluation of Silicon Oxide Films. *J. Electrochem. Soc.*, Vol.122, pp.1013-1019

Rinnert, H.; Vergnat, M.; Burneau, A. (2001). Evidence of Light-Emitting Amorphous Silicon Clusters Confined in a Silicon Oxide Matrix. *J. Appl. Phys.* Vol. 89, No. 1, pp. 237-243

Rochet, F.; Dufour, G.; Roulet, H.; Pelloie, B.; Perrier, J.; Fogarassy, E.; Slaoui, A. & Froment M. (1988). Modification of SiO Through Room-temperature Plasma Treatments, Rapid Thermal Annealing, and Laser Irradiation in a Nonoxidizing Atmosphere. *Phys. Rev. B.*, Vol.37, No 11, pp. 6468-6477

Salihoglu, O.; Kürüm, U.; Yaglioglu, H.G., Elmali, A.; Aydinli, A. (2011). Femtosecond laser crystallization of amorphous Ge. *J. Appl. Rhys.* Vol.109, pp. 123108-1

Sameshima, T. & Usui, S. (1991). Pulsed Laser-induced Amorphization of Silicon Films. *J. Appl. Phys.*, Vol. 70. No. 3, pp. 1281-1289

Sanditov, D.S. (1976). On the Mechanism of Viscous Flow of Glasses. *Glass Physics and Chemistry.* Vol.2, No.6, pp. 515-518

Sheglov, D.V.; Gorokhov, E.B.; Volodin, V.A.; Astankova, K.N. & Latyshev, A.V. (2008). A Novel Tip-induced Local Electrical Decomposition Method for Thin GeO Films Nanostructuring. *Nanotechnology,* Vol.19, pp. 245302-1-4

Takeoka, S.; Fujii, M.; Hayashi, S. & Yamamoto, K. (1998). Size-dependent Near-infrared Photoluminescence From Ge Nanocrystals Embedded in SiO_2 Matrices. *Phys. Rev. B.*, Vol.58, pp. 7921-7925

Tananaev, I. V.; Shpirt, M. Ya. (1967). The Chemistry of Germanium. Khimiya, Moscow (in Russian).

Tyurnina, A.E.; Shur, V.Ya.; Kuznetsov, D.K.; Mingaliev, E.A. & Kozin, R.V. (2011). Synthesis of Silver Nanoparticles by Laser Ablation in Liquid, *Proceedings of 19th International Symposium "Nanostructures: Physics and Technology",* pp. 111-112, ISBN 978-5-93634-042-0, Ekaterinburg, Russia, June 20-25, 2011

Volodin, V.A.; Efremov, M.D; Gritsenko, V.A. & Kochubei S. A. (1998). Raman Study of Silicon Nanocrystals Formed in SiN_x Films by Excimer Laser or Thermal Annealing. *J. Appl. Phys. Lett.*, Vol.73, pp. 1212–1214

Volodin, V.A.; Gorokhov, E.B.; Marin, D.V.; Cherkov, A.G.; Gutakovskii, A.K. & Efremov, M.D. (2005). Ge Nanoclusters in GeO_2: Synthesis and Optical Properties. *Solid State Phenomena,* Vol.108-109, pp. 83-90

Volodin, V.A.; Korchagina, T.T.; Kamaev, G.N.; Antonenko, A.Kh.; Koch, J.; Chichkov, B.N. (2010). Femtosecond and Nanosecond Laser Assistant Formation of Si Nanoclusters in Silicon-Rich Nitride Films. *Proceedings of International Conference "Micro- and Nanoelectronics"*, pp. 75210X1-(X8), SPIE, Vol. 7521, Zvenigorod, Moscow region, Russia, October 5-9, 2009.

Zabotnov, S.V.; Golovan', L.A.; Ostapenko, I.A.; Ryabchikov, Yu.V.; Chervyakov, A.V.; Timoshenko, V.Yu.; Kashkarov, P.K. & Yakovlev, V.V. (2006). Femtosecond Nanostructuring of Silicon Surfaces. *JETP Letters,* Vol. 83, No. 2, pp. 69-71

Zakis, Yu.R. (1981). Applicability of Ideas about *Quasi-Particles and Defects* to *Glass*. *Glass Physics and Chemistry.* Vol.7, No.4, pp. 385-390